

Excited-state DMRG made simple with FEAST

Alberto Baiardi, Anna Klára Kelemen, and Markus Reiher*

*ETH Zürich, Laboratorium für Physikalische Chemie, Vladimir-Prelog-Weg 2, 8093 Zürich,
Switzerland.*

E-mail: markus.reiher@phys.chem.ethz.ch

Abstract

We introduce DMRG[FEAST], a new method for optimizing excited-state many-body wave functions with the density matrix renormalization group (DMRG) algorithm. Our approach applies the FEAST algorithm, originally designed for large-scale diagonalization problems, to matrix product state wave functions. We show that DMRG[FEAST] enables the stable optimization of both low- and high-energy eigenstates, therefore overcoming the limitations of state-of-the-art excited-state DMRG algorithms. We demonstrate the reliability of DMRG[FEAST] by calculating anharmonic vibrational excitation energies of molecules with up to 30 fully coupled degrees of freedom.

1 Introduction

Quantum-chemical formulations of the density matrix renormalization group (DMRG) algorithm^{1–16} have dramatically pushed the limits of full configuration interaction (full-CI) methods in the past two decades. DMRG has opened up the possibility of calculating accurate wave functions for molecular systems including up to 100 particles and orbitals both for electronic^{17–21} and nuclear^{22–27} problems. Unlike approaches that leverage the sparsity of the CI coefficient tensor, such as the full-CI Quantum Monte Carlo^{28,29} algorithm and

selected CI methods,^{30–35} the CI coefficient tensor is replaced with its low-rank tensor-train (TT) factorization^{36,37} in DMRG. The resulting wave function is known as matrix product state (MPS)³⁸ and can be optimized iteratively with the alternating least-squared (ALS) algorithm.³⁷ The combination of MPS and ALS results in the DMRG method. Whereas the quantum-chemical application of DMRG for ground-state many-body wave functions is well established, the design of efficient excited-state DMRG variants still represents a significant challenge. In fact, the area law,³⁹ which ensures that the ground-state wave function of short-ranged Hamiltonians can be encoded as compact MPSs, does not apply to excited states. From a computational perspective, the ALS minimization algorithm relies on the variational principle and is therefore inherently tailored to ground-state calculations. Finally, the number of excited states required for predicting, for instance, molecular spectra in a given energy range can be very large, especially for big systems and for high-energy regions. An excited-state DMRG algorithm that is as efficient as ground-state DMRG and that can target many excited states in parallel is therefore still lacking.

We show, that the algorithm introduced in this work, namely DMRG[FEAST], can fill this gap. DMRG[FEAST] extends the FEAST algorithm^{40–43} to wave functions encoded as MPSs. FEAST is a subspace diagonalization method for generalized eigenvalue problems in which the subspace basis is constructed by approximating the Hamiltonian Green function with a numerical integration of the underlying complex contour integral. The subspace is calculated, in practice, by solving multiple independent linear systems defined in terms of the respective shift-and-invert Hamiltonian.^{22,37,44,45} The present work combines for the first time FEAST and DMRG to design an algorithm that overcomes all the limitations of the existing state-of-the-art excited-state DMRG variants. DMRG[FEAST] is capable of optimizing every state whose energy lies in a given energy interval, which is the only input parameter for the algorithm. This is a major advantage compared to other state-targeting DMRG variants that either require a precise estimate of the excitation energies *a priori*, or rely on root-homing algorithms to follow the target state along with the optimization.^{24,46}

We illustrate the advantages of DMRG[FEAST] for the vibrational formulation of DMRG (vDMRG).^{23,24} Efficient and high-accuracy excited-state methods are particularly relevant for vibrational-structure calculations, where the calculation of anharmonic vibrational spectra with more than 10 atoms requires optimizing hundreds of excited states. We first benchmark the accuracy of DMRG[FEAST] by calculating the vibrational transition frequencies of ethylene.⁴⁷ We demonstrate the reliability of DMRG[FEAST] computing the low-frequency anharmonic vibrations of uracil,⁴⁸ a molecule of 30-modes that is hardly targeted by alternative vibrational CI-based schemes.

2 DMRG for excited states

We first briefly review DMRG theory, both for ground-²³ and excited-²⁴ states, to introduce the basic notation. We then introduce the DMRG[FEAST] algorithm which we apply to the vibrational Hamiltonian described at the end of this section. However, we emphasize that the DMRG[FEAST] algorithm is completely general and can be applied to any Hamiltonian that can be encoded as a matrix product operator (MPO).

2.1 Standard vDMRG

A full-CI wave function of an L -dimensional quantum system reads

$$|\Psi\rangle = \sum_{\sigma_1 \cdots \sigma_L}^{N_{\max}} C_{\sigma_1 \cdots \sigma_L} |\sigma_1 \cdots \sigma_L\rangle = \sum_{\boldsymbol{\sigma}}^{N_{\max}} C_{\boldsymbol{\sigma}} |\boldsymbol{\sigma}\rangle, \quad (1)$$

where the wave function $|\Psi\rangle$ is expressed as a linear combination of occupation number vectors (ONVs) $|\sigma_1 \cdots \sigma_L\rangle$ containing the single-state occupations σ_i . Eq. (1) holds for both electronic and vibrational wave functions, with the respective ONVs defined for an appropriate one-particle basis of up to L one-particle states. In DMRG, the CI tensor $C_{\sigma_1 \cdots \sigma_L}$ is approximated in the TT format,³⁷

$$C_{\sigma_1 \dots \sigma_L} = \sum_{\sigma_1 \dots \sigma_L} \sum_{a_1, \dots, a_{L-1}}^m M_{1,a_1}^{\sigma_1} M_{a_1, a_2}^{\sigma_2} \dots M_{a_{L-1}, 1}^{\sigma_L}. \quad (2)$$

which yields the so-called matrix product state (MPS) wave function *ansatz*.⁴⁹ In Eq. (2) the CI tensor is expressed as a product of L tensors $\{M_{a_{i-1}, a_i}^{\sigma_i}\}$ that are contracted along the auxiliary indices a_i . The maximum value of the auxiliary indices, called the bond dimension m , plays a pivotal role in DMRG. Although an arbitrary full CI wavefunction is represented exactly as an MPS with a bond dimension that grows exponentially with L , low values of m are in practice often sufficient for encoding the ground state of vibrational^{22–24} and electronic^{17,50,51} molecular Hamiltonians.

Analogously, a single-state-driven decomposition of an arbitrary Hamiltonian can be obtained as an MPO:^{7,38}

$$\mathcal{H} = \sum_{\sigma, \sigma'} \sum_{b_1, \dots, b_{L-1}}^r H_{1, b_1}^{\sigma_1, \sigma'_1} \dots H_{b_{L-1}, 1}^{\sigma_L, \sigma'_L} |\sigma\rangle \langle \sigma'|, \quad (3)$$

While the MPS approximates the CI wave function for a fixed value of m , the Hamiltonian is represented exactly by Eq. (3). The sweep-based optimization strategy of DMRG optimizes the MPS representation of the ground state wave function in an iterative fashion. In the single-site variant of DMRG, the energy expectation value is minimized with respect to variation of the $M_{a_{i-1}, a_i}^{\sigma_i}$ tensor. This results in an eigenvalue problem for tensor \mathbf{M}^{σ_i} ,

$$\sum_{b_{i-1}, b_i} \sum_{a'_{i-1}} \sum_{a'_i} \sum_{\sigma'_i} L_{a_{i-1}, a'_{i-1}}^{b_{i-1}} H_{b_{i-1}, b_i}^{\sigma_i, \sigma'_i} R_{a_i, a'_i}^{b_i} M_{a'_{i-1}, a'_i}^{\sigma'_i} = E M_{a_{i-1}, a_i}^{\sigma_i}, \quad (4)$$

where $L_{a_{i-1}, a'_{i-1}}^{b_{i-1}}$ and $R_{a_i, a'_i}^{b_i}$ are the so-called boundaries^{7,52} that collect the partial contraction between the MPS and the MPO for all sites smaller and larger than i , respectively. In single-site DMRG, Eq. (4) is solved one site at a time (in one microiteration step), by increasing i from 1 to L (forward sweep). The optimization is then repeated in the opposite direction, starting from $i=L$ (backward sweep). At each microiteration step, Eq. (4) is solved and the

MPS is updated by selecting the lowest energy root. The sweep optimization may converge to a local minimum of the energy functional, especially in the presence of symmetries in the Hamiltonian. This issue can be addressed with the so-called subspace expansion algorithm⁵³ or by optimizing two consecutive sites simultaneously, which defines the two-site variant of DMRG.⁵²

Several algorithms have been proposed for extending DMRG to excited states.^{24,54–56} The lowest-energy eigenstate can be targeted with conventional DMRG by constraining the optimization to the variational space orthogonal to the ground-state wave function.^{38,52} This procedure can be straightforwardly extended to higher-energy states but since it is inherently sequential, it becomes very inefficient for high-energy states. A more appealing alternative is to apply DMRG to the shift-and-inverted (S&I) counterpart of Eq. (4). The resulting method, DMRG[S&I],²⁴ is more efficient than standard, state-specific DMRG. However, its numerical stability heavily depends on the choice of the shift parameter η and on the root selected at each microiteration step to propagate the boundaries. Root-homing techniques^{24,46,55} were shown to enhance the efficiency of DMRG[S&I], but the optimization remains challenging for high-energy states.

2.2 DMRG[IP]

The DMRG[IP] method combines the Inverse Power (IP) algorithm and DMRG into a method in which, similarly to DMRG[S&I], a single excited state is targeted. However, as opposed to the S&I technique, DMRG[IP] does not require the selection of a root in each microiteration step. Starting from an initial wave function guess $|\Psi_0\rangle$, in each iteration step k of the IP algorithm the S&I operator

$$\Omega_\eta = (\mathcal{H} - \eta\mathcal{I}) \tag{5}$$

is applied to the wave function calculated at the k -th iteration step as

$$|\Psi_k\rangle := (\mathcal{H} - \eta\mathcal{I})^{-1} |\Psi_{k-1}\rangle \quad k = 1, \dots, N_{iter}. \quad (6)$$

The wave function converges to the eigenfunction with energy closest to the shift η for $k \rightarrow +\infty$. In practice, the following equation is solved:

$$\Gamma_\eta |\Psi_k\rangle = |\Psi_{k-1}\rangle, \quad (7)$$

with

$$|\Psi_k\rangle := \frac{|\Psi_k\rangle}{\|\Psi_k\|}, \quad (8)$$

where $\Gamma_\eta = \Omega_\eta^{-1} = (\mathcal{H} - \eta\mathcal{I})$. The solution of Eq. (7), $|\Psi_k\rangle$, defines the right-hand side in the next IP iteration (referred to in the following as ‘‘IP macroiteration’’). The convergence rate of the IP method depends on the following ratio:⁵⁷

$$\rho = \left| \frac{E^{(n)} - \eta}{E^{(n+1)} - \eta} \right|, \quad (9)$$

where $E^{(n)}$ is the target eigenvalue and $E^{(n+1)}$ is the second eigenvalue closest to the shift η . Therefore, fast convergence will be ensured if the shift is chosen close to an exact eigenvalue of \mathcal{H} .

In DMRG[IP], Γ_η is encoded as an MPO and $|\Psi_k\rangle$ is approximated, in each iteration step, as an MPS with a fixed bond dimension m . Since the application of the MPO onto an MPS increases its bond dimension,⁷ the solution to Eq. (7) with DMRG can only be approximate. Following Ref. 22, we approximate the solution to Eq. (7) with the least-squares method. The optimal MPS of a given bond dimension m is then defined by the minimum of the functional $O[\Psi_k]$,^{37,44}

$$\begin{aligned} O_\eta [\Psi_k] &= \|\Gamma_\eta |\Psi_k\rangle - |\Psi_{k-1}\rangle\|^2 \\ &= \langle \Psi_k | \Gamma_\eta^2 | \Psi_k \rangle - 2 \operatorname{Re} \langle \Psi_k | \Gamma_\eta | \Psi_{k-1} \rangle + \langle \Psi_{k-1} | \Psi_{k-1} \rangle \end{aligned} \quad (10)$$

that is calculated with respect to the variation of the MPS site tensors, that is, $\text{argmin}_{M_{a_{i-1},a_i}^{\sigma_i,(k-1)}}(O_\eta[\Psi_k])$. For η values smaller than the smallest eigenvalues of \mathcal{H} , Γ_η is positive definite and the minimum of Eq. (10) is also the minimum of the functional \tilde{O}_η defined as:

$$\tilde{O}_\eta[\Psi_k] = \langle \Psi_k | \Gamma_\eta | \Psi_k \rangle - 2\langle \Psi_{k-1} | \Psi_k \rangle. \quad (11)$$

Γ_η is not positive definite otherwise and the minima of Eq. (10) and (11) do not necessarily coincide. However, Rhakuba and Oseledets argued²² that the equivalence holds in practice for any choice of η , provided that the initial guess for the solution of the linear system is a good approximation of the targeted eigenstate. In DMRG[IP], the functional defined in Eq. (11) is minimized with the ALS algorithm, one site tensor at a time. This is in contrast to standard DMRG, where the variational minimum is defined with respect to the energy expectation value.⁷ By denoting the tensor entering the MPS parametrization of the state $|\Psi_{k-1}\rangle$ for site i as $M_{a_{i-1},a_i}^{\sigma_i,(k-1)}$, and the tensor associated with $|\Psi_k\rangle$ as $M_{a_{i-1},a_i}^{\sigma_i,(k)}$, the first term in Eq. (11) can be written, for site i , as

$$\langle \Psi_k | \Gamma_\eta | \Psi_k \rangle = \sum_{\sigma_i, \sigma'_i} \sum_{\substack{a_{i-1}, a_i \\ a'_{i-1}, a'_i}} \sum_{b_{i-1}, b_i} M_{a_{i-1}, a_i}^{\sigma_i, (k)} L_{a_{i-1}, a'_{i-1}}^{b_{i-1}} G_{b_{i-1}, b_i}^{\sigma_i, \sigma'_i} R_{a_i, a'_i}^{b_i} M_{a'_{i-1}, a'_i}^{\sigma'_i, (k)}, \quad (12)$$

where $G_{b_{i-1}, b_i}^{\sigma_i, \sigma'_i}$ are the tensors defining the MPO representation of Γ_η . The tensors $L_{a_{i-1}, a'_{i-1}}^{b_{i-1}}$ and $R_{a_i, a'_i}^{b_i}$ are the boundaries^{7,52} introduced above. The second term in Eq. (11) can be expressed as

$$\langle \Psi_k | \Psi_{k-1} \rangle = \sum_{\sigma_i} \sum_{a_{i-1}, a_i} \sum_{a'_{i-1}, a'_i} A_{a_{i-1}, a'_{i-1}} M_{a_{i-1}, a_i}^{\sigma_i, (k)} M_{a'_{i-1}, a'_i}^{\sigma_i, (k-1)} B_{a'_i, a_i}, \quad (13)$$

where the tensors $A_{a_{i-1}, a'_{i-1}}$ and $B_{a'_i, a_i}$ collect the partial contractions of the MPSs $|\Psi_{k-1}\rangle$ and $|\Psi_k\rangle$ for sites smaller and larger than i , respectively. By exploiting Eqs. (12) and (13),

the tensor $\tilde{M}_{a_{l-1}, a_l}^{\sigma_l}$ minimizing Eq. (11) is obtained from

$$\sum_{\sigma'_i} \sum_{a'_{i-1}, a'_i} \sum_{b_{i-1}, b_i} L_{b_{i-1}}^{a_{i-1}, a'_{i-1}} G_{b_{i-1}, b_i}^{\sigma_i, \sigma'_i} R_{b_i}^{a_i, a'_i} \tilde{M}_{a'_{i-1}, a'_i}^{\sigma'_i} = \sum_{a'_{i-1}, a'_i} A_{a_{i-1}, a'_{i-1}} \tilde{M}_{\bar{a}_{i-1}, \bar{a}_i}^{\sigma_l} B_{\bar{a}_l, a_l}. \quad (14)$$

Eq. (14) can be recast as a linear system of equations that can be solved with the Generalized Minimal Residual (GMRES) method^{58,59} that solves Eq. (14) in the Krylov space generated by the powers of the Γ_η operator. Note that, in analogy to standard DMRG, the functional defined in Eq. (11) can be minimized with respect to the variation of two neighboring tensors, as is done in the two-site DMRG.^{7,52}

Following Ref. 22, we do not run the DMRG sweeps for solving Eq. (14) until convergence, but rather for a fixed number of sweeps N_{sweeps} . Therefore, we construct the right-hand side of the k -th IP iteration in Eq. (7) from the partially optimized MPS at the $(k-1)$ -th iteration and repeat the procedure until convergence, which is monitored through the parameter λ defined as:

$$\lambda = |\langle \Psi_k | \Psi_{k-1} \rangle|^2. \quad (15)$$

The solution of Eq. (14) is unique, and therefore, DMRG[IP] does not require a root-homing algorithm to select the proper eigenfunction after each microiteration step. However, as for DMRG[S&I], choosing the appropriate η value to target a given eigenstate remains challenging for high-energy states. In the following section, we show that this limitation can be lifted with FEAST.

2.3 DMRG[FEAST]

The FEAST algorithm^{40–43,60} is an iterative subspace diagonalization method for generalized eigenvalue problems. Unlike Davidson-type algorithms,^{61,62} the subspace dimension in FEAST is fixed and the basis in which the diagonalization is carried out is generated by solving a contour integral in the complex plane, for a set of guess vectors. We first introduce the

method as applied to the standard eigenvalue problem and, then, introduce DMRG[FEAST]. Let $I_E = [E_{\min}, E_{\max}]$ be an energy interval that contains M eigenvalues of \mathcal{H} with the corresponding eigenfunctions $I_M = \{\Psi^{(1)}, \dots, \Psi^{(M)}\}$. We consider a closed curve \mathcal{C} in the complex plane enclosing I_E . The projector \mathcal{P}_M associated with I_M can be expressed as a contour integral⁴⁰ based on Cauchy's integral theorem⁶⁰

$$\mathcal{P}_M = \sum_{j=1}^M |\Psi^{(j)}\rangle \langle \Psi^{(j)}| = \frac{1}{2\pi i} \oint_{\mathcal{C}} (z\mathcal{I} - \mathcal{H})^{-1} dz. \quad (16)$$

We apply \mathcal{P}_M onto a set of N linearly independent guess vectors $\{\Phi_{\text{guess}}^{(1)}, \dots, \Phi_{\text{guess}}^{(N)}\}$

$$S_N := \{\mathcal{P}_M \Phi_{\text{guess}}^{(1)}, \dots, \mathcal{P}_M \Phi_{\text{guess}}^{(N)}\}. \quad (17)$$

Eq. (17) corresponds to the subspace basis in which \mathcal{H} is diagonalized in the FEAST algorithm. If N is equal to the number of eigenstates included in I_E , the eigenpairs with eigenvalues within the interval I_E can be obtained. We note that, in practice, overestimating the subspace size by providing $N > M$ guess vectors is necessary to ensure convergence.⁴⁰ This overestimation however, leads to spurious eigenvalues that do not correspond to those of the full Hamiltonian. If the number of guess vectors is $N < M$, the basis S_N does not span the appropriate subspace and the diagonalization does not yield the exact eigenvalues lying in the target interval. Calculating the subspace basis with Eq. (16) would require inverting the $(z\mathcal{I} - \mathcal{H})$ operator and the exact evaluation of the contour integral. The key idea of FEAST is to approximate the complex contour integral with an N_p -point numerical quadrature. Each element of the S_N set is therefore expressed as

$$\mathcal{P}_M \Phi_{\text{guess}}^{(i)} \approx \frac{1}{2\pi i} \sum_{k=1}^{N_p} \omega_k (z_k \mathcal{I} - \mathcal{H})^{-1} \Phi_{\text{guess}}^{(i)} := \sum_{k=1}^{N_p} \omega_k \Phi^{(i,k)}, \quad (18)$$

where ω_k and z_k are nodes and weights defined by the numerical quadrature. The wave function $\Phi^{(i,k)}$ associated with a given quadrature node k and guess i is obtained as solution

of the following linear system:

$$(z_k \mathcal{I} - \mathcal{H}) \Phi^{(i,k)} = \Phi_{\text{guess}}^{(i)}, \quad (19)$$

where $(z_k \mathcal{I} - \mathcal{H}) = -\Omega_{z_k}$, with Ω_{z_k} being the S&I operator defined in Eq. (5). Note that the linear systems defined by Eq. (19) are mutually independent, which makes the FEAST algorithm trivially parallelizable. Each element of S_N is then obtained by evaluating the summation over the quadrature nodes. If Eq. (19) is solved exactly, the only approximation of FEAST is the numeric integration of Eq. (18). In this case FEAST returns the exact eigenpairs in a single iteration for a large enough quadrature grid.

In DMRG[FEAST], we express the initial guess vectors $\{\Phi_{\text{guess}}^{(1)}, \dots, \Phi_{\text{guess}}^{(M)}\}$ as a set of MPSs, each with bond dimension m and Ω_{z_k} associated with each quadrature point in Eq.(19) as an MPO. The solution of Eq. (19), $\Phi^{(i,k)}$, is approximated with the minimum defined by Eq. (14) for an MPS with a fixed bond dimension m . The FEAST subspace basis is obtained by optimizing this MPS with the iterative scheme introduced for DMRG[IP]. Note that the operator appearing in Eq. (19) was introduced for FEAST and has the opposite sign compared to the S&I operator of the DMRG[IP] algorithm. Therefore, the MPO must be scaled by an overall factor of -1 before solving Eq. (19).

Because the sum of two MPSs with bond dimension m is represented by an MPS with bond dimension $2m$,^{22,63} Eq. (18) yields a subspace composed by MPSs with bond dimension $M \times m$.

We therefore expect the MPS representation of the target wave functions associated with I_E to be more accurate than for the original guess states. We report a pseudocode of the DMRG[FEAST] algorithm in Section 3. Note that for Hermitian Hamiltonians Eq.(18) can be rewritten as⁴⁰

$$\begin{aligned}
\mathcal{P}_M \Phi_{\text{guess}}^{(i)} &= \frac{1}{2\pi i} \int_{\mathcal{C}^+} [(z\mathcal{I} - \mathcal{H})^{-1}] \Phi_{\text{guess}}^{(i)} dz + \frac{1}{2\pi i} \int_{\mathcal{C}^-} [(z\mathcal{I} - \mathcal{H})^{-1}] \Phi_{\text{guess}}^{(i)} dz \\
&= \frac{1}{2} \int_0^1 [(z(\theta)\mathcal{I} - \mathcal{H})^{-1} \Phi_{\text{guess}}^{(i)}] \bar{r} e^{i\pi\theta} d\theta - \frac{1}{2} \int_1^0 [(z(\theta)^*\mathcal{I} - \mathcal{H})^{-1} \Phi_{\text{guess}}^{(i)}] \bar{r} e^{-i\pi\theta} d\theta \\
&= \frac{1}{2} \int_0^1 [(z(\theta)\mathcal{I} - \mathcal{H})^{-1}] \Phi_{\text{guess}}^{(i)} \bar{r} e^{i\pi\theta} d\theta + \frac{1}{2} \int_0^1 [(z(\theta)\mathcal{I} - \mathcal{H})^{-1}]^\dagger \Phi_{\text{guess}}^{(i)} \bar{r} e^{-i\pi\theta} d\theta \\
&= \frac{1}{2} \int_0^1 (\Phi^{(i,z)} + \Phi^{(i,z),*}) d\theta
\end{aligned} \tag{20}$$

where \mathcal{C}^+ is the part of the circle lying in the upper positive complex plane, and

$$z(\theta) = \frac{E_{\max} + E_{\min}}{2} + \left(\frac{E_{\max} - E_{\min}}{2} \right) e^{2\pi i \theta}. \tag{21}$$

Eq. (20) expresses $\mathcal{P}_N \Phi_{\text{guess}}^{(i)}$ as a complex integral over the positive half of the complex circle \mathcal{C} . It follows, that for achieving the same accuracy as for a non-Hermitian operator, only half as many quadrature points are needed. In the original FEAST algorithm,⁴⁰ Eq. 20 is further simplified based on the relation $(\Phi^{(i,z)} + \Phi^{(i,z),*}) = 2 \text{Re}(\Phi^{(i,z)})$ that, however, does not hold for MPSs.

Compared to the original FEAST algorithm, DMRG[FEAST] introduces two additional approximations. First, the eigenfunctions of the Hamiltonian are expressed as a linear combination of MPSs with a fixed bond dimension m and, therefore, the energy convergence with respect to the bond dimension must be monitored. Second, we approximate the solutions of Eq. (19) by running the sweep optimization for a finite number of sweeps (N_{sweeps}) and GMRES iteration (N_{GMRES}) and, therefore, approximate the S_N basis. We balance this inaccuracy by repeating the FEAST iteration step for N_{FEAST} iterations. This approach is advantageous because Eq. (19) may be ill-conditioned, especially in energy ranges with a high density of states where a node z_k may be close to an eigenvalue of \mathcal{H} .

We highlight that the number of eigenstates M lying in the interval I_E is not known *a priori*. DMRG[FEAST] must, therefore, be repeated for increasing N_{guess} values to ensure that all

roots are converged.

We assess the convergence of DMRG[FEAST] based on three different criteria. A single microiteration step of a DMRG sweep is converged if the relative residual of the local linear system (Eq. (14)) falls below a given threshold η_{micro} before N_{GMRES} iterations

$$\frac{\mathbf{F}\mathbf{x} - \mathbf{c}}{\mathbf{F}\mathbf{x}_0 - \mathbf{c}} < \eta_{\text{micro}}. \quad (22)$$

where \mathbf{x} is a vector that collects the entries of the $\tilde{M}_{a'_{i-1}, a'_i}^{\sigma'_i}$ tensor, \mathbf{c} collects the entries of the right-hand side Eq. 14, and \mathbf{F} is defined as:

$$F_{(a'_{i-1} a'_i \sigma'_i), (a_{i-1} a_i \sigma_i)} = \sum_{b_{i-1}, b_i} L_{b_{i-1}}^{a_{i-1}, a'_{i-1}} G_{b_{i-1}, b_i}^{\sigma_i, \sigma'_i} R_{b_i}^{a_i, a'_i}. \quad (23)$$

We monitor the convergence of the sweep-based solution of the linear system based on the overlap of the MPS at the current sweep with the MPS obtained at the end of the previous sweep. When this overlap falls below a second threshold η_{overlap} , *i.e.*

$$\text{Re}(|\langle \Psi^k | \Psi^{k-1} \rangle|) < \eta_{\text{overlap}} \quad (24)$$

the MPS is considered stationary and therefore the sweeping procedure is stopped before reaching N_{sweeps} . The convergence of DMRG[FEAST] is assessed following the original implementation of FEAST.⁴⁰ Denoting the eigenvalues at the i -th FEAST iteration as $E^{(i)}$, and $E^{(i+1)}$ the same quantity at the $(i+1)$ -th iteration, the FEAST iterations are stopped if:

$$\frac{\sum_j |E_j^{(i)} - E_j^{(i+1)}|}{\sum_j E_j^{(i)}} < \eta_{\text{FEAST}} \quad (25)$$

η_{FEAST} being a third convergence threshold.

In conclusion, we highlight the advantages of DMRG[FEAST] over DMRG[IP]. The basis of the subspace diagonalization in DMRG[FEAST] is obtained as the target eigenfunctions are obtained in DMRG[IP] for a single iteration. However, the shift in Eq. (19) is determined

by the quadrature defined on the user-defined interval, as opposed to the target energy in Eq. (7) for DMRG[IP]. This is advantageous, since the convergence rate of DMRG[IP] depends on the proximity of the shift to the target state. As we will show in the next section, the selection of I_E is not critical because the interval must merely be sufficiently large to include all target eigenfunctions. As opposed to iteratively improving a single guess by the repeated applications of the shifted operator and, therefore, obtaining the excited state in a sequential fashion as in DMRG[IP], in DMRG[FEAST] multiple independent linear systems corresponding to different quadrature nodes and guesses are solved. Therefore, DMRG[FEAST] can be trivially parallelized at different levels. First, multiple energy regions can be targeted simultaneously with different DMRG[FEAST] runs. Within each run, all linear systems can be solved independently of the others. Finally, the solution of the linear system with DMRG can be parallelized as for conventional DMRG.⁶⁴

2.4 Vibrational DMRG

DMRG[FEAST] can be applied to any Hamiltonian that can be encoded as an MPO. This is the case for electronic,^{52,65,66} vibrational,^{23,25} and rotational⁶⁷ Hamiltonians. In this work, we apply DMRG[FEAST] to the vibrational formulation of DMRG, namely vDMRG.²³ We obtain the MPO representation of the vibrational Hamiltonian of an L -mode system starting from the so-called Watson Hamiltonian expressed in terms of Cartesian normal modes (\mathbf{Q}):^{68,69}

$$\mathcal{H}_{\text{vib}} = - \sum_{i=1}^L \frac{\partial^2}{\partial Q_i^2} + \mathcal{V}(Q_1, \dots, Q_L) \quad (26)$$

and express the potential operator $\mathcal{V}(Q_1, \dots, Q_L)$ with a Taylor expansion around a stationary point of the potential energy surface (PES):

$$\mathcal{V}(Q_1, \dots, Q_L) = \sum_{i=1}^L \omega_i^2 Q_i^2 + \frac{1}{6} \sum_{ijk} k_{ijk} Q_i Q_j Q_k + \frac{1}{24} \sum_{ijkl} k_{ijkl} Q_i Q_j Q_k Q_l. \quad (27)$$

The MPO representation of Eq. 26 based on the potential defined in Eq. 27 is obtained with the algorithm presented in Ref. 23. We encode \mathcal{H}_{vib} in the MPO format by expressing the position operator Q_i and its conjugate momentum P_i in terms of the canonical bosonic second-quantization operators b_i^\dagger, b_i as follows:

$$\begin{aligned} Q_i &= \frac{1}{\sqrt{2}} (b_i^\dagger + b_i) \\ P_i &= \frac{i}{\sqrt{2}} (b_i^\dagger - b_i) \end{aligned} \tag{28}$$

It follows from Eq. 28 that each site i of the DMRG lattice corresponds to a given mode. Harmonic modes fulfill the Bose-Einstein statistics and, therefore, the local dimension of each site (N_{max} in Eq. 2) is unbounded. In practice, we set $N_{\text{max}}=6$ for all calculations since higher energy ONVs give negligible contributions to the final MPS wave function.

3 Computational Details

We outline the DMRG[IP] and DMRG[FEAST] algorithms in Algorithm 1 and 2, respectively. To establish the convergence properties and accuracy of DMRG[IP] and DMRG[FEAST],

Algorithm 1 Pseudocode of the DMRG[IP] algorithm.

- 1: **procedure** SHIFTED INVERSE ITERATION(Ψ_0, η, m)
 - 2: **for** $k = 1, \dots, N_{\text{IP}}$ **do**
 - 3: Solve $(\mathcal{H} - \eta)\Psi_k = \Psi_{k-1}$ where Ψ_k is an MPS with bond dimension m
 - 4: $\Psi_k = \Psi_k / \|\Psi_k\|$
 - 5: **end for**
 - 6: **end procedure**
-

we discuss both methods for the vibrational problem outlined in Section 2.4. We refer to the resulting algorithm as vDMRG[IP] and vDMRG[FEAST], respectively. We note that a DMRG[FEAST] calculation is defined by seven parameters: 1) the bond dimension m , 2) the number of iterations of the iterative linear system solver (N_{GMRES}), 3) the number of microiterations (N_{micro}), 4) the interval for the complex contour integration I_E , 5) the number of quadrature points to approximate the complex contour integral N_p , 6) the number of

Algorithm 2 Pseudocode of the DMRG[FEAST] algorithm.

1: **procedure** DMRG[FEAST]($N_p, m, N_{\text{FEAST}}, N_{\text{GMRES}}, \Phi_0^{(i)}$)
2: **for** $n_{\text{iter}}=0, N_{\text{FEAST}}$ **do**
3: **for** $i=0, N$ **do**
4: **for** $k=0, N_p$ **do**
5: Solve Eq. 19 to calculate $\Phi^{(i,k)}$ as an MPS with bond dimension m .
6: **end for**
7: **end for**
8: Construct the Hamiltonian representation \mathbf{H} in the S_N basis.

$$H_{ij} = \sum_{k,h}^{N_p} \omega_k^* \omega_h \langle \Phi^{(i,k)} | \mathcal{H} | \Phi^{(j,h)} \rangle$$

9: Construct the overlap matrix \mathbf{S} for the S_N basis.

$$S_{ij} = \sum_{k,h}^{N_p} \omega_k^* \omega_h \langle \Phi^{(i,k)} | \Phi^{(j,h)} \rangle$$

10: Solve the generalized eigenvalue problem.

$$\mathbf{H}\mathbf{V}^{n_{\text{iter}}} = \mathbf{E}^{n_{\text{iter}}} \mathbf{S}\mathbf{V}^{n_{\text{iter}}}$$

11: Calculate convergence measure η (Eq. 24)

12: **if** $\eta < \eta_{\text{FEAST}}$ **then**

13: Exit.

14: **else**

15: Construct the guess for next iteration:

16: **for** $i=0, N$ **do**

17:

$$\Phi_{(n_{\text{iter}}+1)}^i = \sum_{k=1}^{N_p} \sum_{j=1}^N V_{i,j} \omega_k \Phi^{(j,k)}$$

18: **end for**

19: **end if**

20: **end for**

21: **end procedure**

MPS guess wave functions, N and 7) the choice for the initial guess MPS. We optimize MPS with the single-site variant of DMRG and set $N_{\text{GMRES}}=50$, unless otherwise specified. We rely on a 8-point Gauss-Hermite quadrature for all vDMRG[FEAST] calculations. Where possible, we compare the vDMRG[IP] and vDMRG[FEAST] results with excited-state energies calculated with the constrained optimization variant of vDMRG (the vDMRG[ortho] method in Ref. 24). We refer to this methods simply as “vDMRG”, for the sake of readability.

A key parameter of both DMRG[FEAST] and DMRG[IP] is the initial guess MPS. In the following, we adopt two choices. We will refer to an MPS where the entries $\mathbf{M}_{a_{i-1}, a_i}^{\sigma_i}$ are initialized randomly $\sigma_i < \sigma_i^{\text{max}}$ as “random guess” ($\sigma_i^{\text{max}} < N_{\text{max}}$ is a mode-specific parameter that is also initialized randomly). The other entries are set to 0. The constraint $\sigma_i < \sigma_i^{\text{max}}$ avoids the generation of guess wave functions corresponding to vibrational states with a large excitation degree that would yield slow convergence rates. Alternatively, we will refer to MPSs constructed from the ONV corresponding to a specific harmonic target state as “harmonic guess”. In all cases, we set $N_{\text{max}} = 6$, *i.e.* we include 6 harmonic basis functions per mode in the MPS wave function.

We applied vDMRG[IP] and vDMRG[FEAST] to two molecular systems: ethylene and uracil. Ethylene is a 12-mode molecule that will serve as a reference to validate the new methods introduced in the present work by comparing them to results obtained by us^{23,24} with the excited-state vDMRG variants introduced in Section 2. Our original work relied on the PES reported in Ref. 47 that we approximated as a sixth-order Taylor expansion with the PyPES software.⁷⁰ Here instead, we rely on the PES reported in Ref. 35 and compare our results with the corresponding vibrational heat-bath CI (vHBCI) calculations. Note that in our previous work on the anharmonic vibrational structure of ethylene²³ we have neglected fifth- and sixth-order force constants smaller than 0.1 cm^{-1} , whereas the PES of Ref. 35 includes the complete sixth-order force field. Small deviations with respect to the data reported in Refs. 23 and 24 are therefore to be expected.

Uracil will serve as a test case to analyse the efficiency of large-scale vDMRG[IP] and vDMRG[FEAST] calculations, for molecules with more than 20 vibrational modes, which are hardly targeted by alternative full CI-based algorithms. We rely on the PES reported in Ref. 48, which is represented as a fourth-order Taylor expansion and includes the full third-order force field, as well as diagonal and semi-diagonal fourth-order force constants. The harmonic frequencies were calculated with Coupled Cluster,⁷¹ while third- and fourth-order anharmonic force constants were calculated with second-order Møller-Plesset perturbation theory.⁷² As already noted in Ref. 48, this PES diverges to large negative energies for large displacements from the equilibrium position. This effect was referred to as PES “holes” in Ref. 48. This divergence affects the accuracy of variational calculations dramatically⁴⁸ since the energy minimization can converge to an unphysical wave function with an energy lower than the ground state. The effect is particularly relevant for vDMRG where the excitation degree of the full CI wave function is not truncated, which leads to the exploration of arbitrarily high-energy configurations. We have removed all anharmonic couplings between the 4 lowest-energy modes and the X-H stretching vibrations and report the resulting PES in the Supplementary Material. In order to assign the optimized excited states obtained with vDMRG[FEAST] or vDMRG[IP], we applied the stochastic reconstruction of the CI wave function introduced in Ref. 73 that we generalized to vibrational wave functions in Ref. 24. This algorithm samples the probability distribution p_{σ} associated with the MPS, defined as

$$p_{\sigma} = \frac{\|C_{\sigma}\|^2}{\sum_{\sigma} \|C_{\sigma}\|^2} \quad (29)$$

by applying the Metropolis-Hastings algorithm. All reported energies are absolute energies and reported in cm^{-1} , if not otherwise specified).

4 Strengths and limitations of vDMRG[IP]

4.1 vDMRG[IP] convergence for ground-state calculations

The key component of both vDMRG[IP] and vDMRG[FEAST] is the solution of linear systems with the DMRG-like algorithm based on the minimization of Eq. (10) with the alternating least squares algorithm. As a first validation step, we analyze the convergence of this algorithm as applied to the vibrational Hamiltonian of ethylene.

Figure 1 depicts the energy convergence of vDMRG[IP] for a single IP iteration ($N_{IP}=1$) such that the initial guess for the MPS defines both the guess for the left- and right-hand side in Eq. (7) for the entire DMRG[IP] run. We optimize the vibrational ground state by choosing the shift just above the expected zero point vibrational energy (ZPVE) of ethylene, $\eta=11000 \text{ cm}^{-1}$. The initial MPS guess is initialized either randomly or as a harmonic guess. For the harmonic guess, the energy converges within 24 microiterations that corresponds to 2 sweeps. The convergence rate is therefore comparable to that of conventional DMRG (upper left panel of Figure 1). If the calculation is initiated from the random guess, vDMRG[IP] converged in approximately 100 microiteration steps, which corresponds to 10 sweeps.

Note that if the guess is an eigenstate of the S&I operator ($\mathcal{H} - \eta\mathcal{I}$), the left- and right-hand side of Eq. (7) match. Given the fact that we construct the guess for the solution of the linear system from the right-hand side MPS, the vDMRG[IP] efficiency is in this case highest. This is the case for the calculations initiated from the harmonic ground-state ONV, but not for these that are started from the default guess. For this reason, the convergence is slower in the latter case. Note that, for the harmonic-guess calculation, DMRG[IP] converges to an energy of 11011.61 cm^{-1} , in good agreement with the vHBCI reference data.³⁵ A single IP macroiteration step is therefore sufficient to converge the ground-state energy of ethylene. This is not the case for the calculations initiated from the random guess that converges to a higher energy of approximately 26500 cm^{-1} . In this case, multiple applications of the S&I operator would be required to converge DMRG[IP], since the overlap of the initial MPS and

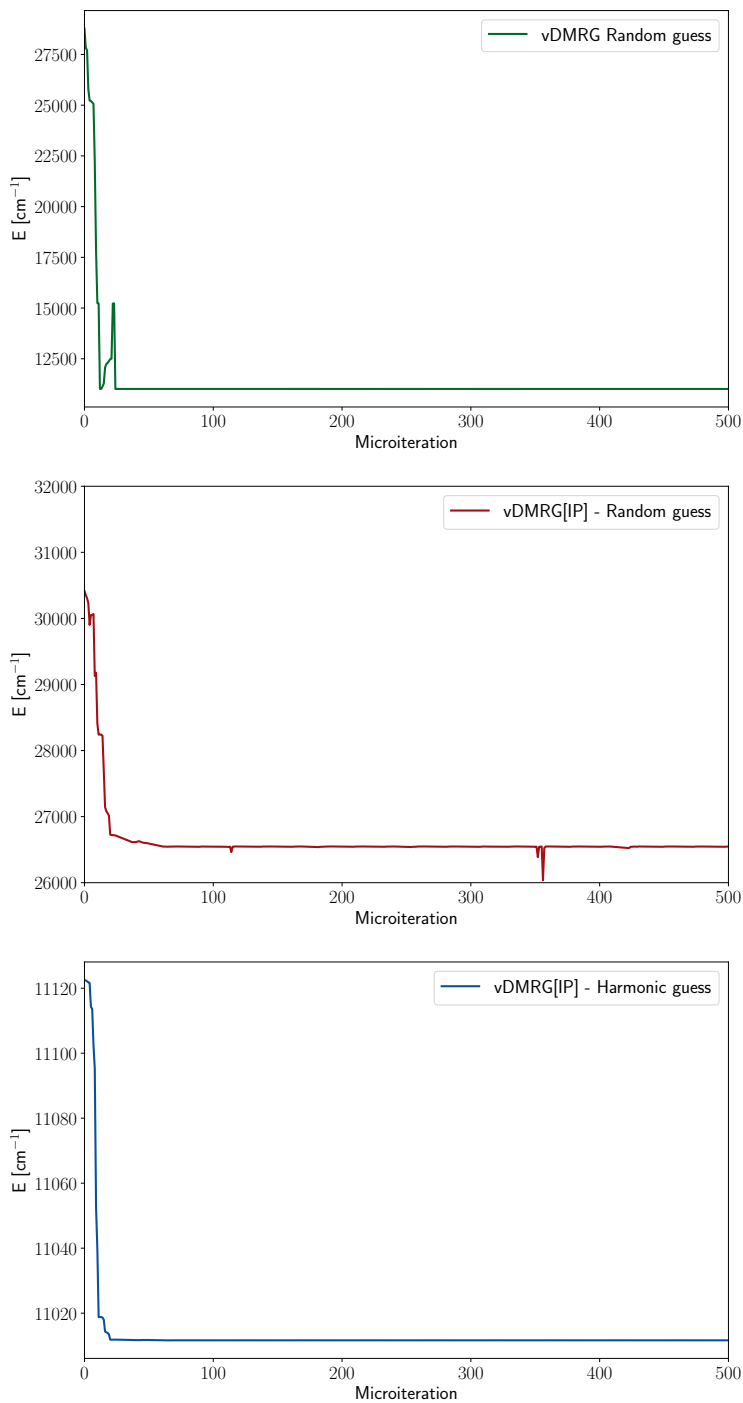


Figure 1: vDMRG (upper panel) and vDMRG[IP] (middle and lower panels) energy convergence for ethylene starting from the same random MPS (upper and center panel) and from the harmonic guess associated with the vibrational ground state (lower panel). In all cases we set $m=50$ and $N_{\text{GMRES}}=50$. For the vDMRG[IP] calculations, we further set $N_{\text{IP}}=1$ and $\eta=11000 \text{ cm}^{-1}$.

the targeted ground state is small.

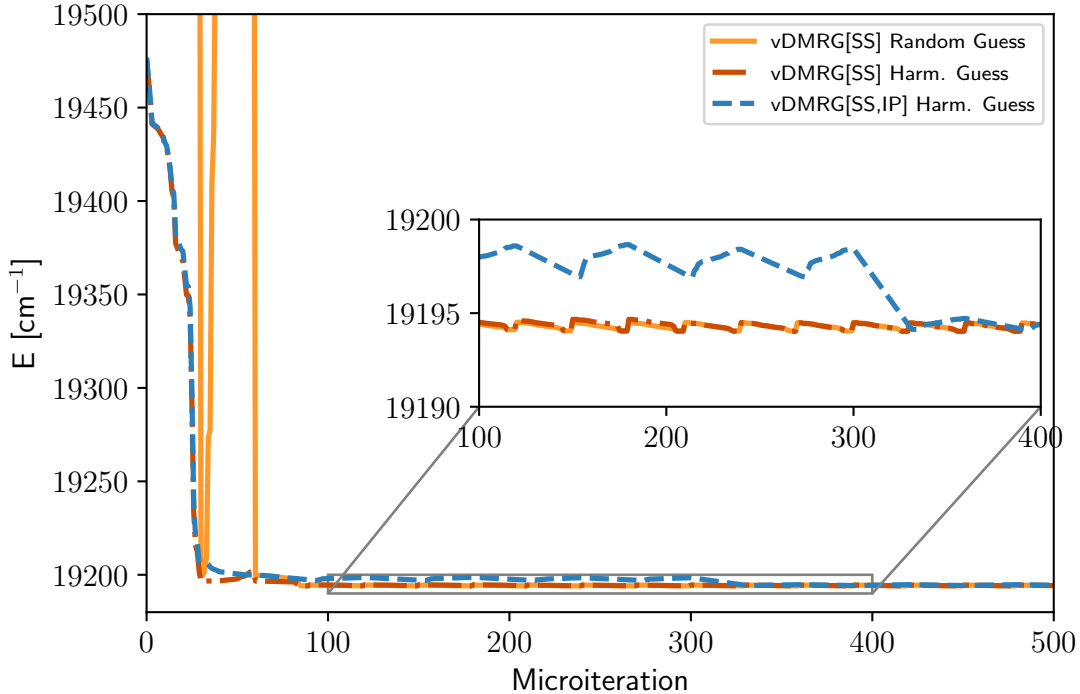


Figure 2: Energy convergence of vDMRG (red lines) and vDMRG[IP] (blue lines) as applied to the optimization of the vibrational ground-state of uracil. We set $\eta=19000\text{ cm}^{-1}$, $m=50$, and $N_{\text{IP}}=5$ for all vDMRG[IP] calculations.

As we show in Figure 2, we observed the same trend also for the larger test case, i.e., for uracil. In this case, we set the shift parameter to 19000 cm^{-1} , an energy value that is lower than the converged vDMRG energy of 19193.96 cm^{-1} . Moreover, we set $N_{\text{IP}}=5$ so that a new IP macroiteration is started after 300 microiterations. As for ethylene, the energy reaches a plateau after 2 sweeps. However, the corresponding energy value is 5 cm^{-1} higher than the converged vDMRG energy. Hence, the solution of the linear system converges after 2 sweeps, but $N_{\text{IP}}=1$ is no longer sufficient to converge the overall vDMRG[IP] calculation.

The previous analysis does not apply to calculations starting from a random MPS guess. As we show in Figure 2, the convergence of vDMRG is almost unchanged compared to the harmonic guess, while the vDMRG[IP] converges only after 8 macroiterations. The vDMRG[IP] convergence is slightly enhanced based on the two-site solver that yields convergence after

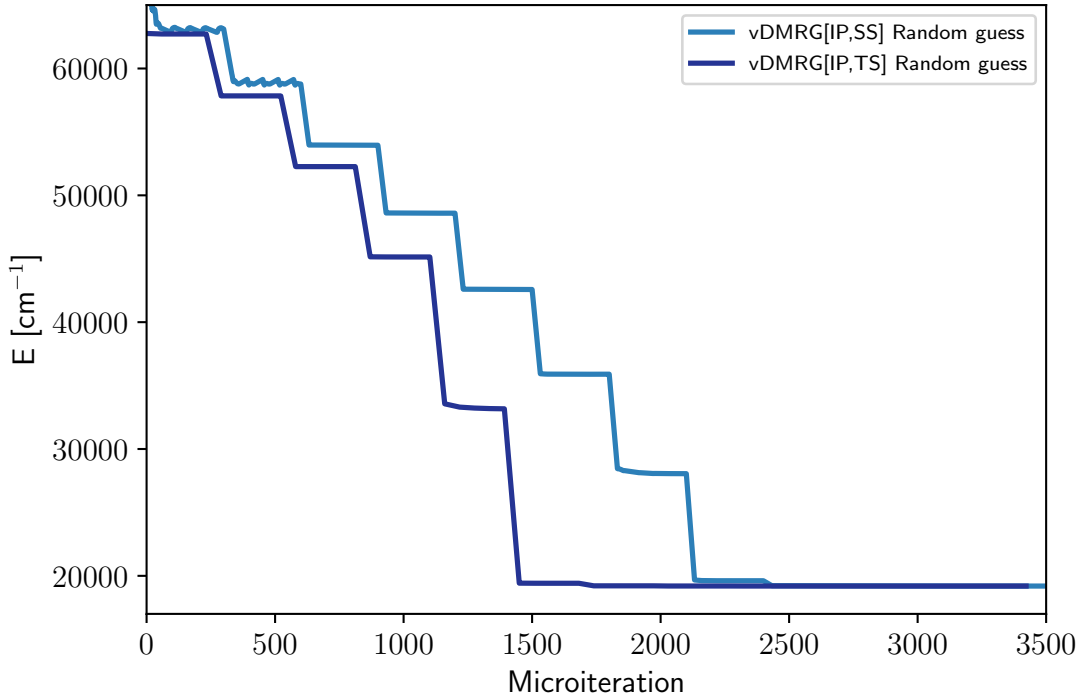


Figure 3: Energy convergence of vDMRG[IP,SS] (dark blue line) and vDMRG[IP,TS] (light blue line) with $\eta=19000 \text{ cm}^{-1}$, $N_{\text{IP}}=5$, $N_{\text{GMRES}} = 50$, and $m=50$.

6 macroiterations. The number of macroiterations required to converge vDMRG[IP] increases by decreasing the overlap of the initial guess with the final, optimized wave function. vDMRG[IP] is therefore less efficient than vDMRG for a generic random guess. We will show later how vDMRG[FEAST] is less dependent on the guess than vDMRG[IP].

4.2 Excited-state targeting with vDMRG[IP]

Although DMRG[IP] can reliably optimize low-energy vibrational states, it becomes completely unfeasible for excited state calculations as we show in Figure 4, where we optimize the vibrational state associated with the symmetric CH stretching mode of ethylene with vDMRG[IP]. The vDMRG[S&I] energy of this state calculated based on the fourth-order Taylor-series-expanded PES was 13982.3 cm^{-1} .²⁴ We therefore chose four shift values η ranging from 13980 cm^{-1} to 14050 cm^{-1} . In all cases, we rely on the harmonic guess. As we show in Figure 4, DMRG[IP] converges within 3 sweeps for $\eta=13990 \text{ cm}^{-1}$ and 14010 cm^{-1} The

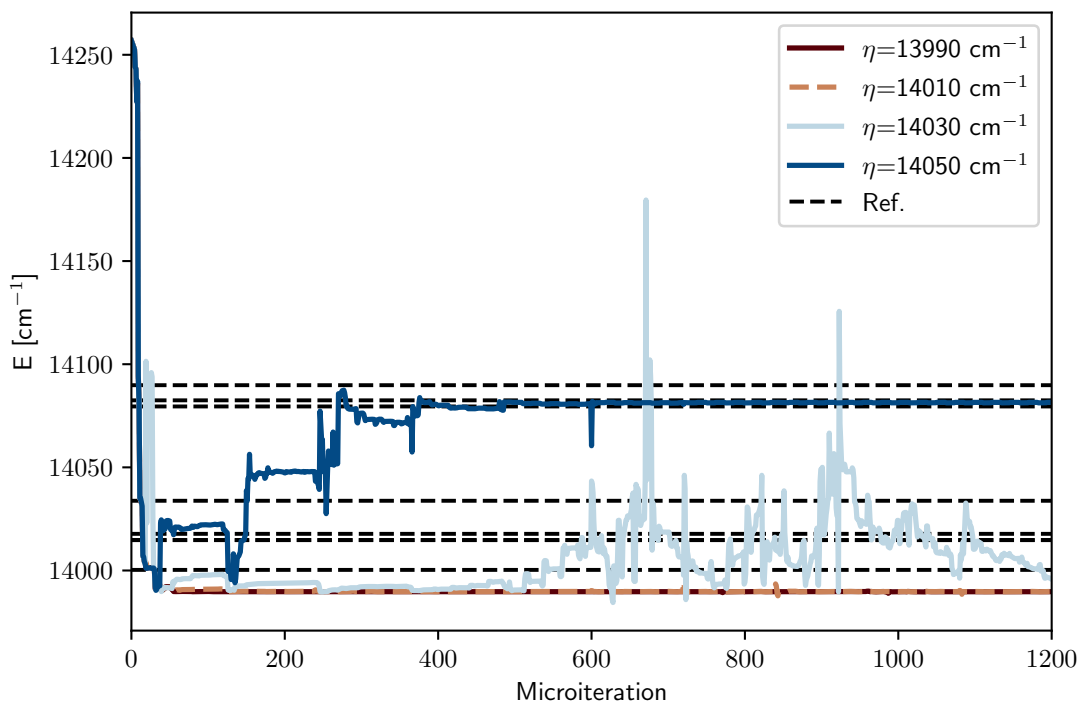


Figure 4: Energy convergence of vDMRG[IP] for ethylene in terms of the number of sweeps obtained with different η values, $m=50$, $N_{\text{GMRES}}=50$, and $N_{\text{IP}}=5$. Selected reference vibrational energies taken from Ref. 47 are represented as horizontal black lines.

converged energy is 13989.72 cm^{-1} , corresponding to an excitation energy of 2978.08 cm^{-1} , in good agreement with the reference VCI energy⁴⁷ of 2985.38 cm^{-1} that is reported in Figure 4 as dashed black line. We note that these VCI energies are calculated for the same PES employed in the present work, but also include vibro-rotational couplings in the Hamiltonian. Therefore, the reference energy is higher by approximately 10 cm^{-1} than the reference one. For $\eta=14030 \text{ cm}^{-1}$, vDMRG[IP] does not converge, while for $\eta=14050 \text{ cm}^{-1}$ it converges to a higher energy of 14081.54 cm^{-1} , corresponding to an excitation energy of 3069.90 cm^{-1} . With the stochastic reconstruction of the CI wave function algorithm^{23,73} we assign this energy to the $\nu_2 + \nu_{12}$ state. The corresponding excitation energy is in good agreement with the VCI reference energy⁴⁷ of 3074.92 cm^{-1} . Therefore, as soon as $\eta=14030 \text{ cm}^{-1}$, i.e. when η falls halfway between the ν_{11} and $\nu_2 + \nu_{12}$ energies, vDMRG[IP] converges the $\nu_2 + \nu_{12}$ state even though the initial guess is the harmonic ν_{11} state. DMRG[IP] convergence is therefore affected by the choice for η , which is independent of the initial guess MPS. We note that vDMRG[IP] energy convergence is enhanced by the point group symmetry of ethylene. In fact, reference VCI data⁴⁷ suggest that 5 states possess an energy higher than that of the ν_{11} state and lower than that of the $\nu_2 + \nu_{12}$ one (we included the corresponding reference energies in Figure 4 as dashed black lines). The vDMRG[IP] optimization scheme does not break the wave function symmetry, and therefore, converges only the states associated with the same irreducible representation as the initial guess MPS, which is the fundamental excitation of the ν_{11} mode and transforms as B_{1u} . The $\nu_2 + \nu_{12}$ combination band is the first state with an energy higher than ν_{11} in symmetry B_{1u} . For this reason, vDMRG[IP] will be unstable starting from $\eta=14030 \text{ cm}^{-1}$. vDMRG[IP] would be even more sensitive to the choice for the shift η for a non-symmetric molecule.

5 Vibrational ground states with vDMRG[FEAST]

We now show that vDMRG[FEAST] can overcome the vDMRG[IP] drawbacks outlined above. We recall that a DMRG[FEAST] calculation is defined by six parameters: 1) the bond dimension m , 2) the number of iterations of the iterative linear system solver (N_{GMRES}), 3) the number of sweeps for the solution of the linear system (N_{sweep}), 4) the interval for the complex contour integration I_E , 5) the number of quadrature points to approximate the complex contour integral, and 6) the number of guesses. These parameters determine the extent to which the subspace basis is approximated. We first apply vDMRG[FEAST] on the energy interval $I_E = [11000, 11100]$ (we report in the following all energies in cm^{-1} if not otherwise specified) for different N_{GMRES} and m values. This interval includes only the vibrational ground state, and therefore, we set $N_{\text{guess}}=1$.

Table 1: vDMRG[FEAST] energy convergence with respect to N_{FEAST} for $E_{\text{min}} = 11000 \text{ cm}^{-1}$, $E_{\text{max}} = 11100 \text{ cm}^{-1}$, $N_{\text{sweep}}=5$, and different m and N_{GMRES} values. All energies are reported in cm^{-1} .

		m	20	20	50	50
		N_{GMRES}	20	50	20	50
Random guess	N_{FEAST}	1	11286.51	14413.97	11326.70	11047.72
		2	10677.59	10794.03	10810.65	11011.66
		3	10999.47	10992.57	10777.01	11011.64
		4	10816.20	11105.86	10995.05	11011.64
Harmonic guess	N_{FEAST}	1	11012.01	11012.01	11011.64	11011.64
		2	11012.01	11012.01	11011.64	11011.64
		3	11012.01	11012.01	11011.64	11011.64
		4	11012.01	11012.01	11011.64	11011.64

We show in Table 1 that, starting from the random guess, vDMRG[FEAST] converges only with $m=50$ and $N_{\text{GMRES}}=50$, whereas convergence is not achieved with lower m and N_{GMRES} values. Conversely, vDMRG[FEAST] converges in a single FEAST iteration when the op-

timization is initiated from the harmonic guess. We approximately solve the linear system with fixed m , N_{GMRES} , and $N_{\text{sweep}}=5$ values, and therefore, approximate the projector \mathcal{P}_M defined in Eq. (16). The impact of this approximation on the vDMRG[FEAST] convergence decreases by increasing the overlap of the guess wave function with the final, exact eigenfunction. The harmonic guess represents more accurately the target state, and hence, it yields faster vDMRG[FEAST] convergence. Finally, we note that the converged vDMRG[FEAST] ground-state energy (11011.64 cm^{-1}) agrees well with the reference energy calculated with heat-bath CI (11011.61 cm^{-1}).³⁵ This suggests that the discrepancy with the energy reported in our original vDMRG work²³ is due to the differences in the potential energy surface mentioned in Section 3.

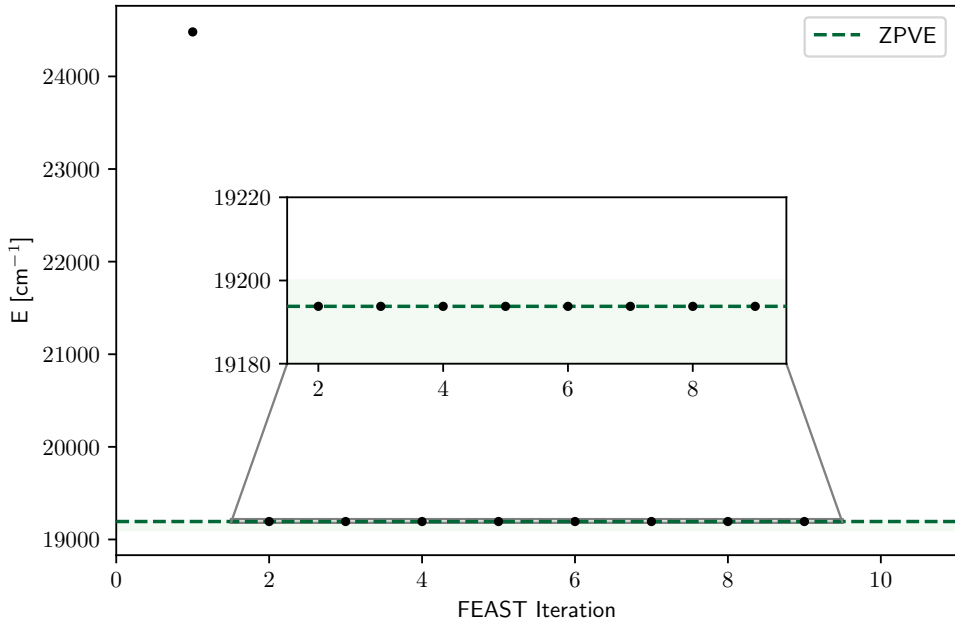


Figure 5: vDMRG[FEAST] energy convergence for the ZPVE of uracil obtained with $E_{\text{min}}=19100 \text{ cm}^{-1}$, $E_{\text{max}}=19200 \text{ cm}^{-1}$, $N_{\text{GMRES}}=50$, $N_{\text{sweep}}=5$, $m=50$, N_{guess} , starting from the random guess. The reference energy obtained by us for this work with vDMRG is reported as a dashed black line.

We now apply the optimal parameter set, $m=50$ and $N_{\text{GMRES}}=50$, to optimize the vibrational ground state of uracil. We report in Figure 5 the vDMRG[FEAST] energy convergence obtained starting from the random guess. Even though the initial guess does not approximate

the final wave function, vDMRG[FEAST] converges in 2 FEAST macroiteration steps, as opposed to vDMRG[IP] that converges, as shown in Figure 3, in 9 iterations. This confirms that vDMRG[FEAST] is less sensitive to the choice for the initial guess.

6 Excited-state optimization with vDMRG[FEAST]

In this section, we first apply vDMRG[FEAST] to optimize low- and high-energy vibrational states of ethylene to highlight how vDMRG[FEAST] convergence changes with the density of states of the targeted energy interval. Then, we optimize the low-energy excited states of uracil with vDMRG[FEAST] to demonstrate its reliability for large molecules.

6.1 vDMRG[FEAST]: optimization of low-lying excited states

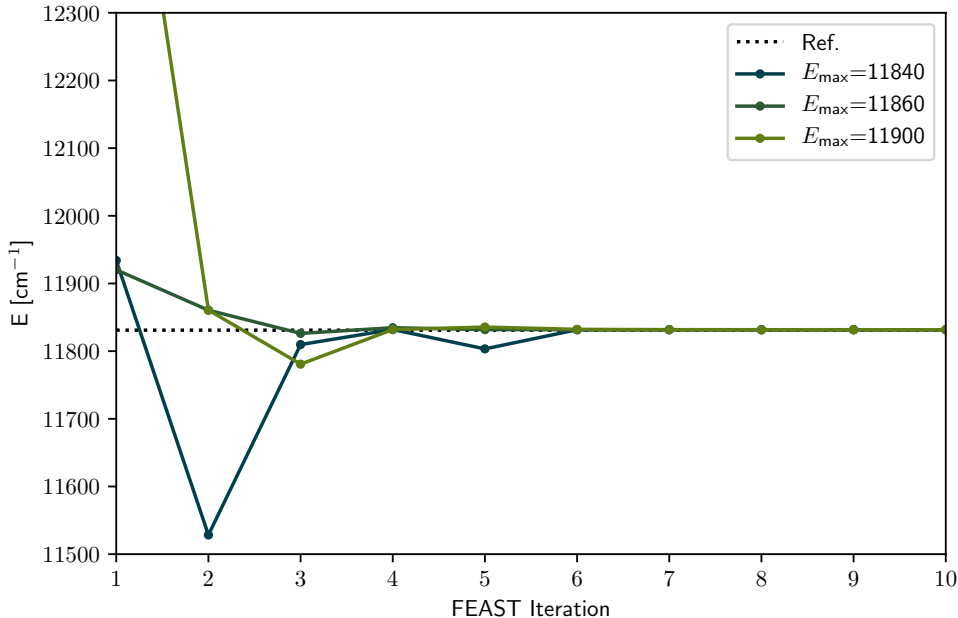


Figure 6: vDMRG[FEAST] energy convergence for the first excited state of ethylene obtained with $N_{\text{GMRES}}=50$, $N_{\text{IP}}=10$, $N_{\text{guess}}=2$, $m=50$, $E_{\text{min}}=11820 \text{ cm}^{-1}$ and changing E_{max} values. The reference energy 'Ref.' (dotted black line) was calculated by us for this work with vDMRG[ortho] and is 11831.58 cm^{-1} .

Figure 6 shows the vDMRG[FEAST] energy convergence obtained with $E_{\text{min}}=11820 \text{ cm}^{-1}$

and E_{\max} values ranging from 11840 cm^{-1} to 11900 cm^{-1} starting from random MPSs. Reference energies, reported in Table 2 and calculated with vDMRG,²⁴ indicate that I_E includes only the first excited vibrational state for all E_{\max} values. Even though vDMRG[FEAST] should, in principle, converge that vibrational state already with $N_{\text{guess}}=1$, we follow Ref. 40 and set $N_{\text{guess}}=2$ to enhance algorithm convergence. In all cases, vDMRG[FEAST] converges in 6 iterations to an energy value that matches the vDMRG reference value (see Table 2) indicating that the integration interval I_E has only a minor effect on vDMRG[FEAST] convergence. Moreover, Figure 6 confirms that the linear system can be safely solved by minimizing Eq. (11) also for η values that are larger than the smaller eigenvalue of \mathcal{H}_{vib} .

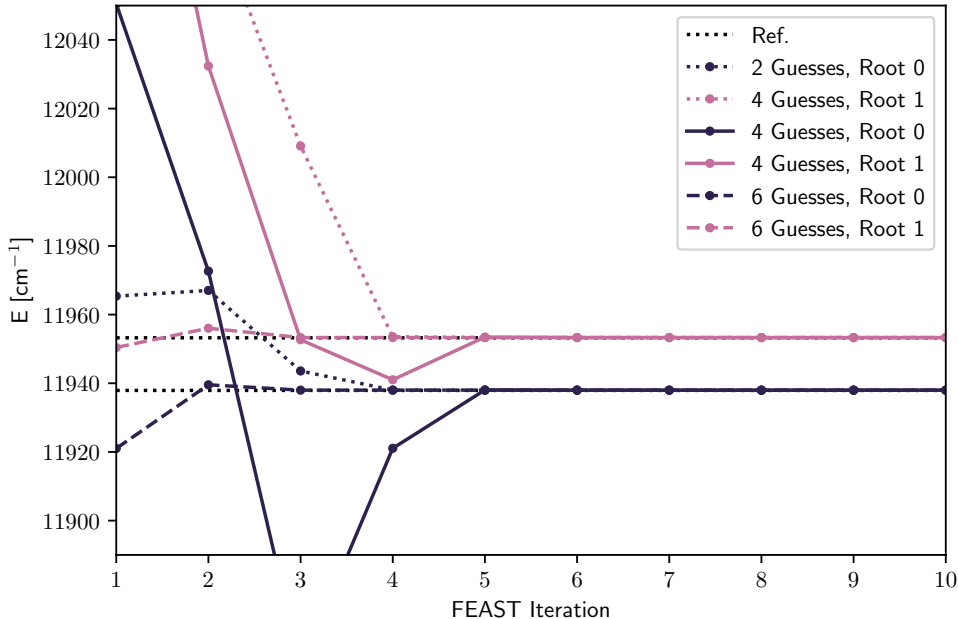


Figure 7: vDMRG[FEAST] energy of the second (purple lines) and third (pink lines) excited states of ethylene obtained with $N_{\text{guess}}=2$ (dotted lines), $N_{\text{guess}}=4$ (solid lines), and $N_{\text{guess}}=6$ (dashed lines). In all cases, we set $N_{\text{GMRES}}=50$, $N_{\text{sweep}}=5$, $m=50$, $E_{\min}=11920 \text{ cm}^{-1}$, and $E_{\max}=11960 \text{ cm}^{-1}$ and started the optimization from random MPSs. The reference energies 'Ref.' (dotted black lines) were calculated by us for this work with vDMRG[ortho] and $m=100$. They are 11937.92 cm^{-1} and 11953.24 cm^{-1} , respectively.

The choice for N_{guess} becomes less trivial for energy regions with a higher density of states. We show in Figure 7 vDMRG[FEAST] energy convergence for $E_{\min}=11920 \text{ cm}^{-1}$ and $E_{\max}=11960 \text{ cm}^{-1}$, an energy interval that includes the second and third excited vibrational state (see Table 2).

Hence, N_{guess} must be larger than 2 to converge all states included in this energy interval. As shown in Figure 7, both energies are converged after 5 FEAST iteration steps with $N_{\text{guess}}=4$ and in 2 FEAST macroiteration steps with $N_{\text{guess}}=6$. Therefore, if the initial guess is not an accurate approximation to the target wave function, increasing N_{guess} and, hence, the subspace size, will enhance DMRG[FEAST] convergence.

6.2 Parallel exploration of different energy regions

Table 2: vDMRG[FEAST] energy of ethylene obtained for varying m values, $N_{\text{guess}}=8$, $N_{\text{sweep}}=5$, $N_{\text{GMRES}}=50$ for three energy intervals $I_1 = [11800, 12000]$, $I_2 = [12000, 12400]$, $I_3 = [12400, 12800]$. All energies are given in cm^{-1} . vDMRG reference data were calculated by us for this work with the constrained optimization excited-state vDMRG[ortho] variant. For comparison, the last column collects vHBCI data taken from Ref. 35.

E_{min}	E_{max}	State	vDMRG[FEAST]			vDMRG	Ref. 35
			$m=20$	$m=50$	$m=100$		
11800	12000	1	11831.93	11831.60	11831.58	11831.58	11831.60
		2	11938.23	11937.94	11937.92	11937.92	11937.94
		3	11953.56	11953.26	11953.24	11953.24	11953.26
12000	12400	4	12029.36	12029.06	12029.05	12029.04	12029.06
		5	12234.03	12233.76	12233.71	12233.75	12233.77
		6	12353.88	12353.55	12353.53	12353.53	12353.56
12400	12800	7	12450.31	12449.93	12449.91	12449.90	12449.92
		8	12634.71	12634.05	12633.95	12633.95	12634.39
		9	12666.10	12665.00	12664.93	12664.93	12666.82
		10	12760.39	12759.67	12759.59	12759.63	12759.66
		11	12778.39	12777.81	12777.75	12777.76	12777.80

An appealing, key feature of vDMRG[FEAST] is that different energy regions can be explored independently of one another. We illustrate this by optimizing the complete set of excited states of ethylene with a vibrational energy lower than 12800 cm^{-1} . We partition the energy

spectrum into three regions, $I_1=[11800 \text{ cm}^{-1}, 12000 \text{ cm}^{-1}]$, $I_2=[12000 \text{ cm}^{-1}, 12400 \text{ cm}^{-1}]$, and $I_3=[12400 \text{ cm}^{-1}, 12800 \text{ cm}^{-1}]$, and apply vDMRG[FEAST] to each interval. In principle, the number of excited states in each energy interval could be estimated based on reference VCI data.⁴⁷ However, accurate reference energies are not, in general, available for large molecules that are the ultimate target of vDMRG[FEAST]. Therefore, we set $N_{\text{guess}}=8$ for all energy intervals, which overestimates the number of states included in each interval, and start the vDMRG[FEAST] optimization from random MPSs. We show in Table 2 that vDMRG[FEAST] and vDMRG energies agree up to 0.01 cm^{-1} for all states. Small deviations, in all cases smaller than 1 cm^{-1} , are observed compared to reference heat-bath CI energies.³⁵ The largest deviation is observed for the 8-th excited state, where the reference energy is higher than the vDMRG[FEAST] one by about 0.44 cm^{-1} . However, the agreement with the vDMRG data suggests that the discrepancy is due to a partial convergence of the vHBCI calculation.

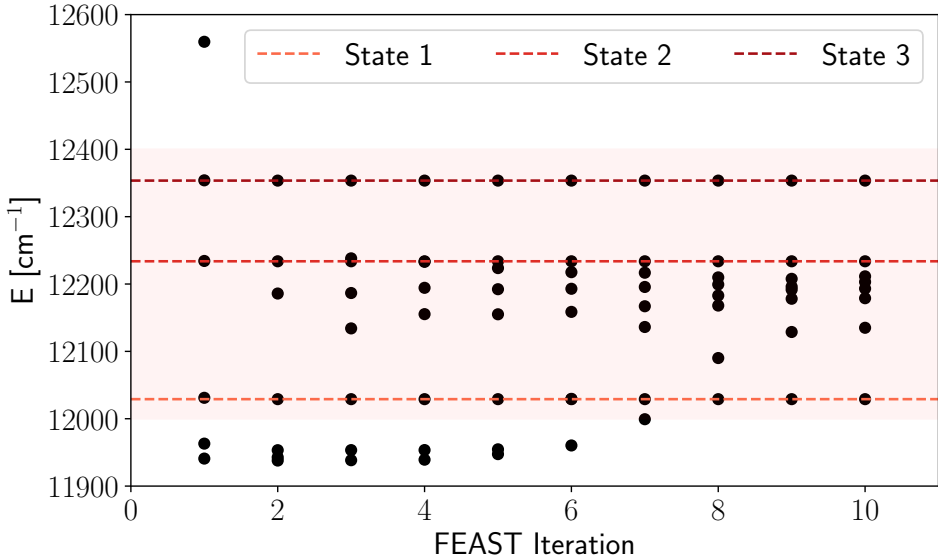


Figure 8: vDMRG[FEAST] energies obtained with $N_{\text{GMRES}}=50$, $N_{\text{sweep}}=50$, $m=50$, $N_{\text{guess}}=8$ and for the energy intervals $I_2=[12000 \text{ cm}^{-1}, 12400 \text{ cm}^{-1}]$ (upper panel) and $I_3=[12400 \text{ cm}^{-1}, 12800 \text{ cm}^{-1}]$ (lower panel). The colored bands represent the energy values included in the I_2 and I_3 intervals, respectively. Reference energies, taken from the vDMRG column of Table 2, are represented as dashed black lines.

We analyze in Figure 8 vDMRG[FEAST] energy convergence for the I_2 and I_3 energy intervals. For I_2 , all three states converge already at the first iteration, even though the optimization is started from randomly initialized MPSs. Conversely, two iterations are required to converge all states in the I_3 interval. As for the conventional FEAST algorithm,⁴⁰ also the vDMRG[FEAST] convergence rate increases with the ratio between N_{guess} and the number of states included in I_E . Note also that, if N_{guess} is larger than the number of states included in I_E , some of the roots returned by the subspace diagonalization will correspond to states that do not approximate eigenstates of \mathcal{H}_{vib} . This is the case for all MPSs whose energy is not included in the I_E interval. Then, we calculate the variance for all remaining states based on the algorithm introduced in Ref. 24 and identify all MPSs with a variance smaller than 100 cm^{-1} as “physically acceptable” states.

6.3 Efficient targeting of high-energy vibrations

So far, we have applied vDMRG[FEAST] to energy ranges associated with a low density of states. These intervals can be efficiently targeted also with alternative excited-state vDMRG variants.²⁴ We show now that vDMRG[FEAST] can calculate with the same efficiency also the excitation energy of the four high-energy fundamental transitions of the C-H stretching vibration of ethylene.

For highly-excited states it is difficult, if not impossible, to select the energy interval I_E so that it includes only a given, target state. This renders the choice for I_E and N_{guess} extremely challenging. We propose a three-step computational procedure to automate the selection of the N_{guess} and I_E parameters in vDMRG[FEAST]. We first obtain an estimate of the energy of the target vibrational state ($E_{\text{approx}}^{\text{target}}$), either from the harmonic approximation or cost-efficient approximate anharmonic methods, such as second-order vibrational perturbation theory.⁷⁴ We then apply vDMRG[FEAST] to an interval $I_E^{(1)}$ centered around $E_{\text{approx}}^{\text{target}}$. The convergence of vDMRG[FEAST] is ensured only if $I_E^{(1)}$ includes the energy of the target state ($E_{\text{VCI}}^{\text{target}}$), and therefore, if the interval size is larger than the accuracy of the $E_{\text{approx}}^{\text{target}}$

estimate. In this first step we truncate the PES and include only four-body operator in order to limit the MPO size, and hence, the computational cost. This first vDMRG[FEAST] calculation yields a second, more accurate energy estimate, $E_{\text{FEAST},1}^{\text{target}}$. Finally, we apply vDMRG[FEAST] on an interval $I_E^{(2)}$ centered around the $E_{\text{FEAST},1}^{\text{target}}$ with the full, six-body potential. $E_{\text{FEAST},1}^{\text{target}}$ is a much more accurate approximation of the exact energy compared to $E_{\text{approx}}^{\text{target}}$ and, therefore $I_E^{(2)}$ should include, ideally, only the target energy.

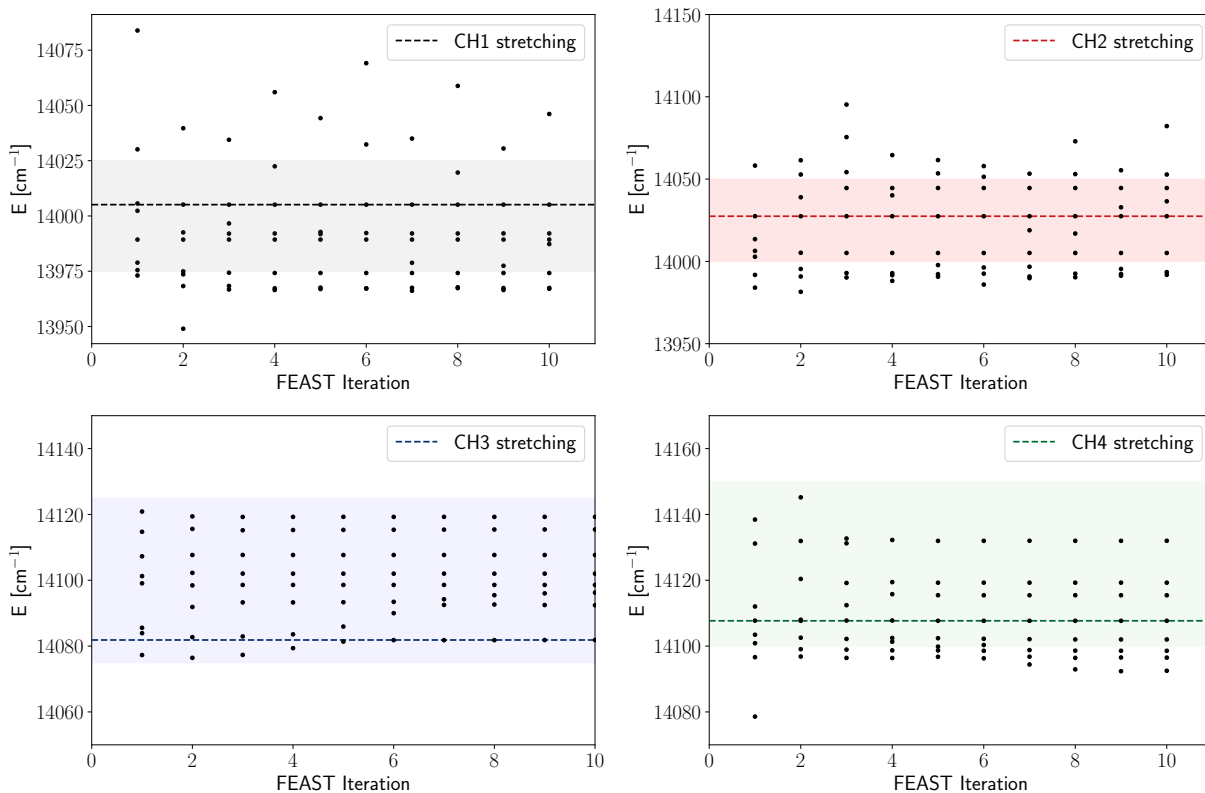


Figure 9: vDMRG[FEAST] energy convergence for the fundamental excitation of the first (upper left panel), second (upper right panel), third (lower left panel), and fourth (lower right panel) C-H stretching mode. We set the energy interval to $E_{\text{min}}=13975 \text{ cm}^{-1}$ and $E_{\text{max}}=14025 \text{ cm}^{-1}$ (upper left panel), $E_{\text{min}}=14000 \text{ cm}^{-1}$ and $E_{\text{max}}=14050 \text{ cm}^{-1}$ (upper right panel), $E_{\text{min}}=14075 \text{ cm}^{-1}$ and $E_{\text{max}}=14125 \text{ cm}^{-1}$ (lower left panel), and $E_{\text{min}}=14100 \text{ cm}^{-1}$ and $E_{\text{max}}=14150 \text{ cm}^{-1}$ (lower right panel). In all cases, we set $N_{\text{GMRES}}=50$, $m=50$, $N_{\text{quad}}=8$, and $N_{\text{guess}}=8$. We report the final, converged energies of the target state with a black dashed line.

Instead of relying on approximate anharmonic vibrational-structure calculation for the first step, we obtain $E_{\text{approx}}^{\text{target}}$ from the VCI data of Ref. 47 and set the size of $I_E^{(1)}$ to 50 cm^{-1} ,

to mimic the inaccuracy of the reference data. Figure 9 exhibits the vDMRG[FEAST] convergence of the first vDMRG[FEAST] calculation phase for the fundamental excitation of the four C-H vibrations (labelled in the following as CH1, CH2, CH3, and CH4, in increasing energy order). In all cases, we rely on $N_{\text{guess}}=8$ guess MPSs, the harmonic one and 7 random guesses. We identified the target state among the N_{guess} MPSs returned by DMRG[FEAST] based on the stochastic reconstruction of the CI wave function algorithm introduced above.⁷³ The calculated results are given in Figure 9 and in Table 3. Note that, even though $N_{\text{guess}}=8$ in all cases, the number of final eigenvalues included in the target interval changes with I_E and ranges from 2, for the CH2 mode, to 8, for the CH3 and CH4 modes. The latter calculations could be repeated with a larger N_{guess} value to ensure that all eigenstates included in I_E are converged. However, this is not necessary because this first calculation step returns only an energy estimate for the second, more accurate vDMRG[FEAST] calculation phase.

Table 3: vDMRG[FEAST] energies of four C-H stretching modes of ethylene calculated based on the four-body PES and an interval $I_E^{(1)}$ with size 50 cm^{-1} , and with the full six-body potential and an interval $I_E^{(2)}$ with size 10 cm^{-1} . The vDMRG[FEAST] parameters are $N_{\text{GMRES}}=50$, $m=50$, $N_{\text{quad}}=8$, and $N_{\text{sweep}}=5$. VCI reference energies taken from Ref. 47 are given for comparison. All energies are reported in cm^{-1} .

PES	N_{guess}	CH1	CH2	CH3	CH4
4 body	8	13989.32	14027.44	14081.85	14107.68
6 body	1	13989.85	14027.75	14082.78	14103.20
	4	13989.64	14028.03	14082.78	14103.10
VCI ⁴⁷		14000.29	14033.90	14094.77	14116.16

We run this second set of vDMRG[FEAST] calculations with an interval I_E centered on the energies reported in Table 3, with $|E_{\text{max}} - E_{\text{min}}| = 10 \text{ cm}^{-1}$ and varying N_{guess} values. As expected, the vDMRG[FEAST] convergence with N_{guess} is faster for this smaller energy interval, and a reliable estimate of the vibrational energies is already obtained with $N_{\text{guess}}=1$ with variations below 1 cm^{-1} obtained with $N_{\text{guess}}=4$. Note that the reference VCI energies⁴⁷

are consistently lower compared to the vDMRG[FEAST] results by approximately 10 cm^{-1} . As already noted above, such a discrepancy is to be expected since we neglected vibro-rotational couplings, which are instead included in the VCI calculation of Ref. 47.

6.4 Towards large-scale vDMRG[FEAST]: uracil

Finally, we demonstrate the reliability of vDMRG[FEAST] for large-scale anharmonic calculations. We optimize the 11 lowest-energy excited states of our second benchmark molecule, uracil. Table 4 contains the vDMRG[FEAST] energies obtained with $m=50$ and 100, together with reference data obtained with vDMRG.

Table 4: vDMRG[FEAST] energies of the 11 lowest-energy vibrational states of uracil calculated with $N_{\text{GMRES}}=50$, $N_{\text{quad}}=8$, and varying I_E and m values. Reference data taken from Ref. 48 are given for comparison. All calculations are based on the harmonic guess.

I_E	State	$m=50$	$m=100$	Ref. 48	vDMRG($m=50$)
[19200, 19300]	ZPVE	19218.45		18969.21	19193.19
	1	146.30	147.28	140.02	147.58
[19300, 19500]	2	164.49	165.50	157.09	165.83
	3	292.03	292.65	294.53	293.46
	4	312.87	311.98	385.15	312.91
[19500, 19600]	5	331.27	330.45	379.36	331.31
	6	386.62	386.32	510.81	386.53
	7	419.81	419.34	535.08	419.80
	8	437.33	435.89	543.15	437.34
[19600, 19700]	9	457.97	456.28	542.77	457.98
	10	477.62	475.99	528.68	520.01
	11	496.19	494.73	651.91	477.64

Following the same strategy adopted for ethylene, we partition the energy region in three regions, $I_1=[19300 \text{ cm}^{-1}, 19500 \text{ cm}^{-1}]$, $I_2=[19500 \text{ cm}^{-1}, 19600 \text{ cm}^{-1}]$, and $I_3=[19600 \text{ cm}^{-1}, 19700 \text{ cm}^{-1}]$. In view of the results discussed above, we enhanced the vDMRG[FEAST] convergence by starting the optimization from the harmonic guess in all cases. Table 4 also provides the energies obtained with vDMRG. Both vDMRG and vDMRG[FEAST] converge the energy of all vibrational states below 1 cm^{-1} already with $m=50$, therefore confirming that molecular anharmonic vibrational wave functions can be encoded as com-

pact MPSs. Moreover, even though the vDMRG[FEAST] energies consistently match their vDMRG counterpart, state swappings are observed. For instance, the energy of the 10-th state is higher than that of the 11-th one. Root swapping effects largely affect the efficiency of vDMRG, especially for nearly-degenerate high-energy states. This is not the case of vDMRG[FEAST], however, which calculates each state independently of the others and not in a sequential fashion.

7 Conclusions

In this work, we introduced the DMRG[FEAST] algorithm to efficiently optimize excited states of high-dimensional, many-body Hamiltonians, represented as matrix product states. DMRG[FEAST] applies the FEAST algorithm⁴⁰ to wave functions and operators encoded as matrix product states and matrix product operators, respectively.³⁸ We show that DMRG[FEAST] overcomes the main limitations of the existing excited state DMRG algorithms.^{24,52,54–56} First, it enables optimizing all the eigenfunctions with an energy lying in a given energy interval without the need of estimating *a priori* the energy of the target excited states. Moreover, it does not require calculating powers of the Hamiltonian, which are difficult to encode as compact matrix product operators.^{24,75} Finally, all DMRG[FEAST] calculation steps are trivially parallelizable, which makes DMRG[FEAST] particularly appealing for large-scale excited-state calculation.

We applied DMRG[FEAST] to the optimization of high-energy vibrationally excited states of molecular systems with the vibrational DMRG algorithm, although it can be applied to other quantum chemical problems (e.g., in electronic structure theory) equally well. Vibrational-structure calculations are, however, the perfect application target for DMRG[FEAST] because calculating vibrational spectra requires obtaining many excitation energies. We benchmarked the accuracy of DMRG[FEAST] on ethylene against VCI reference data.⁴⁷ Then, we applied DMRG[FEAST] to calculate the anharmonic vibrational energies of uracil, a system

that is a major challenge for state-of-the-art full configuration-interaction methods.⁴⁸ Our future work will focus on further enhancing the DMRG[FEAST] generality and efficiency. Here, we applied vDMRG[FEAST] to optimize specific vibrational states, such as the fundamental excitation energy of the C-H stretching modes of ethylene and the low-energy excited states of uracil. However, DMRG[FEAST] can be straightforwardly extended to optimize all the excited states in a given energy interval by partitioning it into multiple sub-intervals and applying DMRG[FEAST] to each of them. Each energy subinterval can be targeted independently from the others, and therefore, the overall algorithm can be trivially parallelized. Work is currently in progress in our group on automating DMRG[FEAST] based on such a strategy. The application of DMRG[FEAST] to electronic structure calculations will be particularly appealing for calculating high-energy core-excited states that are difficult to target with conventional multi-configurational methods. The resulting algorithm would enable the calculation of X-ray spectra beyond the linear response⁷⁶ and the state-averaged restricted active space⁷⁷ approximations. Finally, we note that DMRG[FEAST] is not tailored to a specific tensor network parameterization and can be extended to the optimization of multi-dimensional tensor network states.⁷⁸

Acknowledgement

This work was supported by ETH Zürich through the ETH Fellowship No. FEL-49 18-1. The authors gratefully acknowledge Dr. Andrea Muolo (Hebrew University of Jerusalem) for fruitful discussions about the FEAST algorithm.

References

- (1) White, S. R. Density matrix formulation for quantum renormalization groups. *Phys. Rev. Lett.* **1992**, *69*, 2863–2866.

- (2) White, S. R. Density-matrix algorithms for quantum renormalization groups. *Phys. Rev. B* **1993**, *48*, 10345–10356.
- (3) Legeza, Ö.; Noack, R. M.; Sólyom, J.; Tincani, L. Applications of quantum information in the density-matrix renormalization group. *Lect. Notes Phys.* **2008**, *739*, 653–664.
- (4) Chan, G. K.-L.; Dorando, J. J.; Ghosh, D.; Hachmann, J.; Neuscamman, E.; Wang, H.; Yanai, T. *Front. Quantum Syst. Chem. Phys.*; 2008; pp 49–65.
- (5) Chan, G. K. L.; Zgid, D. The Density Matrix Renormalization Group in Quantum Chemistry. *Annu. Rep. Comput. Chem.* **2009**, *5*, 149–162.
- (6) Marti, K. H.; Reiher, M. The density matrix renormalization group algorithm in quantum chemistry. *Z. Phys. Chem.* **2010**, *224*, 583–599.
- (7) Schollwöck, U. The density-matrix renormalization group in the age of matrix product states. *Ann. Phys.* **2011**, *326*, 96–192.
- (8) Chan, G. K.-L.; Sharma, S. The Density Matrix Renormalization Group in Quantum Chemistry. *Annu. Rev. Phys. Chem.* **2011**, *62*, 465–481.
- (9) Wouters, S.; Van Neck, D. The density matrix renormalization group for ab initio quantum chemistry. *Eur. Phys. J. D* **2013**, *31*, 395–402.
- (10) Kurashige, Y. Multireference electron correlation methods with density matrix renormalisation group reference functions. *Mol. Phys.* **2014**, *112*, 1485–1494.
- (11) Olivares-Amaya, R.; Hu, W.; Nakatani, N.; Sharma, S.; Yang, J.; Chan, G. K.-L. The ab-initio density matrix renormalization group in practice. *J. Chem. Phys.* **2015**, *142*, 34102.
- (12) Szalay, S.; Pfeffer, M.; Murg, V.; Barcza, G.; Verstraete, F.; Schneider, R.; Legeza, Ö. Tensor product methods and entanglement optimization for ab initio quantum chemistry. *Int. J. Quantum Chem.* **2015**, *115*, 1342–1391.

- (13) Yanai, T.; Kurashige, Y.; Mizukami, W.; Chalupský, J.; Lan, T. N.; Saitow, M. Density matrix renormalization group for ab initio calculations and associated dynamic correlation methods: A review of theory and applications. *Int. J. Quantum Chem.* **2015**, *115*, 283–299.
- (14) Knecht, S.; Hedegård, E. D.; Keller, S.; Kovyshin, A.; Ma, Y.; Muolo, A.; Stein, C. J.; Reiher, M. New Approaches for ab initio Calculations of Molecules with Strong Electron Correlation. *Chimia* **2016**, *70*, 244–251.
- (15) Freitag, L.; Reiher, M. *Quantum Chemistry and Dynamics of Excited States*; John Wiley & Sons, Ltd, 2020; Chapter 7, pp 205–245.
- (16) Baiardi, A.; Reiher, M. The density matrix renormalization group in chemistry and molecular physics: Recent developments and new challenges. *J. Chem. Phys.* **2020**, *152*, 040903.
- (17) Marti, K. H.; Ondík, I. M.; Moritz, G.; Reiher, M. Density matrix renormalization group calculations on relative energies of transition metal complexes and clusters. *J. Chem. Phys.* **2008**, *128*, 014104.
- (18) Kurashige, Y.; Chan, G. K.-L.; Yanai, T. Entangled quantum electronic wavefunctions of the Mn₄CaO₅ cluster in photosystem II. *Nat. Chem.* **2013**, *5*, 660–666.
- (19) Kurashige, Y.; Saitow, M.; Chalupsky, J.; Yanai, T.; Chalupskyá, J.; Chalupskyá, C.; Yanai, T. Radical O–O coupling reaction in diferrate-mediated water oxidation studied using multireference wave function theory. *Phys. Chem. Chem. Phys.* **2014**, *16*, 11988.
- (20) Sharma, S.; Sivalingam, K.; Neese, F.; Chan, G. K.-L. Low-energy spectrum of iron-sulfur clusters directly from many-particle quantum mechanics. *Nat. Chem.* **2014**, *6*, 927–933.

- (21) Sinha, S. B.; Shopov, D. Y.; Sharninghausen, L. S.; Stein, C. J.; Mercado, B. Q.; Balcells, D.; Pedersen, T. B.; Reiher, M.; Brudvig, G. W.; Crabtree, R. H. Redox Activity of Oxo-Bridged Iridium Dimers in an N,O-Donor Environment: Characterization of Remarkably Stable Ir(IV,V) Complexes. *J. Am. Chem. Soc.* **2017**, *139*, 9672–9683.
- (22) Rakhuba, M.; Oseledets, I. Calculating vibrational spectra of molecules using tensor train decomposition. *J. Chem. Phys.* **2016**, *145*, 124101.
- (23) Baiardi, A.; Stein, C. J.; Barone, V.; Reiher, M. Vibrational Density Matrix Renormalization Group. *J. Chem. Theory Comput.* **2017**, *13*, 3764–3777.
- (24) Baiardi, A.; Stein, C. J.; Barone, V.; Reiher, M. Optimization of highly excited matrix product states with an application to vibrational spectroscopy. *J. Chem. Phys.* **2019**, *150*, 094113.
- (25) Muolo, A.; Baiardi, A.; Feldmann, R.; Reiher, M. Nuclear-electronic all-particle density matrix renormalization group. *J. Chem. Phys.* **2020**, *152*, 204103.
- (26) Feldmann, R.; Muolo, A.; Baiardi, A.; Reiher, M. Quantum Proton Effects from Density Matrix Renormalization Group Calculations. *Arxiv e-prints* **2021**, 2109.05377.
- (27) Glaser, N.; Baiardi, A.; Reiher, M. Tensor Network States for Vibrational Spectroscopy. **2021**, arXiv:2109.08961
- (28) Booth, G. H.; Thom, A. J. W.; Alavi, A. Fermion Monte Carlo without fixed nodes: A game of life, death, and annihilation in Slater determinant space. *J. Chem. Phys.* **2009**, *131*, 54106.
- (29) Cleland, D. M.; Booth, G. H.; Alavi, A. A study of electron affinities using the initiator approach to full configuration interaction quantum Monte Carlo. *J. Chem. Phys.* **2011**, *134*, 24112.

- (30) Huron, B.; Malrieu, J. P.; Rancurel, P. Iterative perturbation calculations of ground and excited state energies from multiconfigurational zeroth-order wave functions. *J. Chem. Phys.* **1973**, *58*, 5745–5759.
- (31) Tubman, N. M.; Lee, J.; Takeshita, T. Y.; Head-Gordon, M.; Whaley, K. B. A deterministic alternative to the full configuration interaction quantum Monte Carlo method. *J. Chem. Phys.* **2016**, *145*, 044112.
- (32) Schriber, J. B.; Evangelista, F. A. Communication : An adaptive configuration interaction approach for strongly correlated electrons with tunable accuracy. *J. Chem. Phys.* **2017**, *144*, 161106.
- (33) Smith, J. E. T.; Mussard, B.; Holmes, A. A.; Sharma, S. Cheap and Near Exact CASSCF with Large Active Spaces. *J. Chem. Theory Comput.* **2017**, *13*, 5468–5478.
- (34) Li, J.; Otten, M.; Holmes, A. A.; Sharma, S.; Umrigar, C. J. Fast semistochastic heat-bath configuration interaction. *J. Chem. Phys.* **2018**, *149*, 214110.
- (35) Fetherolf, J. H.; Berkelbach, T. C. Vibrational heat-bath configuration interaction. *J. Chem. Phys.* **2021**, *154*, 074104.
- (36) Kolda, T. G.; Bader, B. W. Tensor Decompositions and Applications. *SIAM Rev.* **2009**, *51*, 455–500.
- (37) Oseledets, I. V.; Dolgov, S. V. Solution of Linear Systems and Matrix Inversion in the TT-Format. *SIAM J. Sci. Comput.* **2012**, *34*, A2718–A2739.
- (38) Muth, D.; McCulloch, I. P. From density-matrix renormalization group to matrix product states. *J. Stat. Mech. Theory Exp.* **2007**, *2007*, P10014.
- (39) Hastings, M. B. An area law for one-dimensional quantum systems. *J. Stat. Mech. Theory Exp.* **2007**, *2007*, P08024–P08024.

- (40) Polizzi, E. Density-matrix-based algorithm for solving eigenvalue problems. *Phys. Rev. B* **2009**, *79*, 115112.
- (41) Tang, P. T. P.; Polizzi, E. Feast as a subspace iteration eigensolver accelerated by approximate spectral projection. *SIAM J. Matrix Anal. Appl.* **2014**, *35*, 354–390.
- (42) Güttel, S.; Polizzi, E.; Tang, P. T. P.; Viaud, G. Zolotarev quadrature rules and load balancing for the FEAST eigensolver. *SIAM J. Sci. Comput.* **2015**, *37*, A2100–A2122.
- (43) Kestyn, J.; Polizzi, E.; Tang, P. T. P. FEAST eigensolver for non-Hermitian problems. *SIAM J. Sci. Comput.* **2016**, *38*, S772–S799.
- (44) Holtz, S.; Rohwedder, T.; Schneider, R. The alternating linear scheme for tensor optimization in the tensor train format. *SIAM J. Sci. Stat. Comput.* **2012**, *34*, A683–A713.
- (45) Savostyanov, D. V.; Dolgov, S. V.; Werner, J. M.; Kuprov, I. Exact NMR simulation of protein-size spin systems using tensor train formalism. *Phys. Rev. B* **2014**, *90*, 85139.
- (46) Butscher, W.; Kammer, W. Modification of Davidson’s method for the calculation of eigenvalues and eigenvectors of large real-symmetric matrices: “Root Homing Procedure”. *J. Comp. Chem.* **1976**, *20*, 313–325.
- (47) Delahaye, T.; Nikitin, A.; Rey, M.; Szalay, P. G.; Tyuterev, V. G. A new accurate ground-state potential energy surface of ethylene and predictions for rotational and vibrational energy levels. *J. Chem. Phys.* **2014**, *141*, 104301.
- (48) Thomas, P. S.; Carrington, T.; Agarwal, J.; Schaefer, H. F. Using an iterative eigensolver and intertwined rank reduction to compute vibrational spectra of molecules with more than a dozen atoms: Uracil and naphthalene. *J. Chem. Phys.* **2018**, *149*, 064108.
- (49) Rommer, S.; Östlund, S. Class of ansatz wave functions for one-dimensional spin systems and their relation to the density matrix renormalization group. *Phys. Rev. B* **1997**, *55*, 2164–2181.

- (50) Chan, G. K.-L.; Head-Gordon, M. Highly correlated calculations with a polynomial cost algorithm: A study of the density matrix renormalization group. *J. Chem. Phys.* **2002**, *116*, 4462–4476.
- (51) Legeza, Ö.; Röder, J.; Hess, B. A. QC-DMRG study of the ionic-neutral curve crossing of LiF. *Mol. Phys.* **2003**, *101*, 2019–2028.
- (52) Keller, S.; Dolfi, M.; Troyer, M.; Reiher, M. An efficient matrix product operator representation of the quantum chemical Hamiltonian. *J. Chem. Phys.* **2015**, *143*, 244118.
- (53) Hubig, C.; McCulloch, I. P.; Schollwöck, U.; Wolf, F. A. Strictly single-site DMRG algorithm with subspace expansion. *Phys. Rev. B* **2015**, *91*, 155115.
- (54) Dorando, J. J.; Hachmann, J.; Chan, G. K.-L. Targeted excited state algorithms. *J. Chem. Phys.* **2007**, *127*, 84109.
- (55) Devakul, T.; Khemani, V.; Pollmann, F.; Huse, D. A.; Sondhi, S. L. Obtaining highly excited eigenstates of the localized XX chain via DMRG-X. *Philos. Trans. R. Soc. A* **2017**, *375*, 20160431.
- (56) Yu, X.; Pekker, D.; Clark, B. K. Finding Matrix Product State Representations of Highly Excited Eigenstates of Many-Body Localized Hamiltonians. *Phys. Rev. Lett.* **2017**, *118*, 17201.
- (57) Saad, Y. *Numerical Methods for Large Eigenvalue Problems*; Manchester University Press, 2011.
- (58) Saad, Y.; Schultz, M. H. GMRES: A Generalized Minimal Residual Algorithm for Solving Nonsymmetric Linear Systems. *SIAM J. Sci. Stat. Comput.* **1986**, *7*, 856–869.
- (59) Koch, T.; Liesen, J. The conformal ‘bratwurst’ maps and associated Faber polynomials. *Numer. Math.* **2000**, *86*, 173–191.

- (60) Galgon, M.; Krämer, L.; Lang, B. The FEAST algorithm for large eigenvalue problems. *PAMM* **2011**, *11*, 747–748.
- (61) Davidson, E. R. The iterative calculation of a few of the lowest eigenvalues and corresponding eigenvectors of large real-symmetric matrices. *J. Comput. Phys.* **1975**, *17*, 87–94.
- (62) Sleijpen, G. L. G.; Van Der Vorst, H. A. A Jacobi-Davidson Iteration Method for Linear Eigenvalue Problems. *SIAM J. Matrix Anal. Appl.* **1996**, *17*, 401–425.
- (63) Guo, S.; Li, Z.; Chan, G. K.-L. A Perturbative Density Matrix Renormalization Group Algorithm for Large Active Spaces. *J. Chem. Theory Comput.* **2018**, *14*, 4063–4071.
- (64) Brabec, J.; Brandejs, J.; Kowalski, K.; Xantheas, S.; Legeza, O.; Veis, L. Massively parallel quantum chemical density matrix renormalization group method. *J. Comp. Chem.* **2021**, *42*, 534–544.
- (65) Chan, G. K.-L.; Keselman, A.; Nakatani, N.; Li, Z.; White, S. R. Matrix product operators, matrix product states, and ab initio density matrix renormalization group algorithms. *J. Chem. Phys.* **2016**, *145*, 014102.
- (66) Battaglia, S.; Keller, S.; Knecht, S. Efficient Relativistic Density-Matrix Renormalization Group Implementation in a Matrix-Product Formulation. *J. Chem. Theory Comput.* **2018**, *14*, 2353–2369.
- (67) Iouchtchenko, D.; Roy, P. N. Ground states of linear rotor chains via the density matrix renormalization group. *J. Chem. Phys.* **2018**, *148*, 134115.
- (68) Watson, J. K. G. Simplification of the molecular vibration-rotation Hamiltonian. *Mol. Phys.* **1968**, *15*, 479–490.
- (69) Papousek, D.; Aliev, M. R. In *Molecular Vibrational-rotational Spectra: Theory and*

Applications of High Resolution Infrared, Microwave and Raman Spectroscopy of Polyatomic Molecules; Ltd, E. S., Ed.; 1982.

- (70) Sibae, M.; Crittenden, D. L. The PyPES library of high quality semi-global potential energy surfaces. *J. Comput. Chem.* **2015**, *36*, 2200–2207.
- (71) Puzzarini, C.; Biczysko, M.; Barone, V. Accurate Anharmonic Vibrational Frequencies for Uracil: The Performance of Composite Schemes and Hybrid CC/DFT Model. *J. Chem. Theory Comput.* **2011**, *7*, 3702–3710.
- (72) Krasnoshchekov, S. V.; Vogt, N.; Stepanov, N. F. Ab Initio Anharmonic Analysis of Vibrational Spectra of Uracil Using the Numerical-Analytic Implementation of Operator Van Vleck Perturbation Theory. *J. Phys. Chem. A* **2015**, *119*, 6723–6737.
- (73) Boguslawski, K.; Marti, K. H.; Reiher, M. Construction of CASCI-type wave functions for very large active spaces. *J. Chem. Phys.* **2011**, *134*.
- (74) Barone, V. Anharmonic vibrational properties by a fully automated second-order perturbative approach. *J. Chem. Phys.* **2005**, *122*, 014108.
- (75) Mach, T. Computing Inner Eigenvalues of Matrices in Tensor Train Matrix Format. *Numerical Mathematics and Advanced Applications 2011*. Berlin, Heidelberg, 2013; pp 781–788.
- (76) Nakatani, N.; Wouters, S.; Van Neck, D.; Chan, G. K.-L. Linear response theory for the density matrix renormalization group: Efficient algorithms for strongly correlated excited states. *J. Chem. Phys.* **2014**, *140*, 024108.
- (77) Guo, M.; Sørensen, L. K.; Delcey, M. G.; Pinjari, R. V.; Lundberg, M. Simulations of iron K pre-edge X-ray absorption spectra using the restricted active space method. *Phys. Chem. Chem. Phys.* **2016**, *18*, 3250–3259.

- (78) Larsson, H. R. Computing vibrational eigenstates with tree tensor network states (TTNS). *J. Chem. Phys.* **2019**, *151*, 204102.